NRL Report 6800

# The NRL SOLRAD 9 Satellite Solar Explorer B 1968-17A

R. W. Kreplin and D. M. Horan

*E. O. Hulburt Center for Space Research*
*Space Science Division*

March 24, 1969

**NAVAL RESEARCH LABORATORY**
**Washington, D.C.**

This document has been approved for public release and sale; its distribution is unlimited.

CONTENTS


Abstract ii
Problem Status ii
Authorization ii

INTRODUCTION 1

THE EXPERIMENTS 4

SPACECRAFT DESCRIPTION 7

DESCRIPTION OF THE SOLRAD 9 EXPERIMENTS 10

The Aspect System 10
Primary 1 to 8 Å X-Ray Photometer Experiment 11
Primary 8 to 16 Å Photometer Experiment 14
0.5 to 3 Å Ion Chamber and Geiger Counter Experiments 18
1 to 8 Å Geiger Counter Experiment 21
Scintillation Counter Experiment for Solar X-Rays 40 to 80 and 20 to 80 kev 23
Ultraviolet Ionization Chamber Experiments 26
1 to 20 Å and 44 to 60 Å X-Ray Photometer Experiments 27
Experiment Status Commutator 31

EXPERIMENT BLOCK DIAGRAM AND ANALOG OUTPUT FORMAT 31

CONVERSION OF CURRENT OR COUNTING RATE TO FLUX VALUES 31

NOTE ON ANGULAR RESPONSE CORRECTIONS 32

ACKNOWLEDGMENTS 38

APPENDIX A -- Correction of 44 to 60 Å Photometer Response for Radiation in the Wavelength Region Below 20 Å 39

APPENDIX B -- Correction to Phase and Amplitude of Photometer Signals for Spin Rate 44

## ABSTRACT

The NRL SOLRAD 9 satellite, launched March 5, 1968, carried instruments to measure solar radiation in the x-ray region from 0.1 to 60 Angstroms and in the far-ultraviolet from 1080 to 1350 Angstroms. These special regions are covered by a number of band-sensitive ionization-chamber photometers, Geiger counters, and scintillation counters. These bands are: 20 to 80 kev (0.15 to 0.6 Å); 40 to 80 kev (0.15 to 0.3 Å); 0.5 to 3 Å; 1 to 8 Å; 8 to 16 Å; 1 to 20 Å; 44 to 60 Å; 1080 to 1350 Å; and 1225 to 1350 Å. An aspect sensor was also included to measure the angle between the solar direction and view direction of the photometers for correction of photometer measurements in case of failure of the attitude-control system.

The satellite transmits its x-ray and ultraviolet measurements in real time via an FM/AM telemetry system operating in the 136-MHz band. The standard IRIG subcarrier channels 3 through 8 carry the output of the various photometers and associated housekeeping data.

Individual scientists and institutions have been invited through COSPAR to receive and use the real-time transmission of x-ray and ultraviolet measurements in their own research programs.

This report carries a full description of each instrument aboard the SOLRAD 9 spacecraft and all calibration data required to reduce the telemetered measurements to x-ray and ultraviolet flux values.


## PROBLEM STATUS

This is an interim report on one phase of the problem; work on this and other phases is continuing.

## AUTHORIZATION


NRL Problem A01-20
Project A37538/6521/F019-02-02

Manuscript submitted August 28, 1968.

# THE NRL SOLRAD 9 SATELLITE
# SOLAR EXPLORER B
# 1968-17A

## INTRODUCTION

The NRL SOLRAD 9 satellite is a continuation of a program whose purpose is to make continuous measurements of the sun's x-ray emission. The first satellite in this series was designated 1960 eta 2 and was launched in June 1960.

The last three satellites in the series have been highly successful — 1964-01D, 1965-16D, and 1965-93A (SOLRAD 8). With these spacecraft, solar x-ray radiation has been monitored nearly continuously since January 1964. The minimum flux levels at the lowest part of the sunspot cycle have been determined, and numbers of emission events have been observed in two or more x-ray bands in the increasing phase of the current solar cycle.

In those spacecraft launched before SOLRAD 8, the data were telemetered only in real time, so the data were interrupted when the satellite was beyond the range of telemetry receiving stations of the NASA STADAN network. SOLRAD 8 carried a data-storage system to bridge these gaps; however, due to thermal problems, it operated for only a month. The satellite continued transmitting in real time and provided almost two years of reliable solar monitoring.

Every malfunction of SOLRAD 8 has been carefully studied. Where required, corrections have been made in components and design of SOLRAD 9.

The SOLRAD 9 satellite was launched by a NASA Scout rocket from Wallops Island, Virginia, at 1828 UT on Mar. 5, 1968. Its international designation is 1968-17A.

SOLRAD 9 is the first of the SOLRAD series to depart in its external configuration from the early Vanguard design. This departure has been dictated by the successful use of attitude control in SOLRAD 8 and a requirement for greater power to operate experiments. The spacecraft (Fig. 1) is essentially in the shape of a 12-sided drum, 30 in. long and about 30 in. in diameter. The experiment photometers are located in the 12 faces of the satellite, in an equatorial band about 8 in. high. Above and below this band are skirts on which the silicon solar cells are mounted.

The satellite transmits its solar x-ray and ultraviolet data in real time by means of an FM/AM telemetry system operating in the 136-MHz telemetry band. The standard IRIG subcarrier channels 3 through 8 are used for transmission of the solar data and for housekeeping functions.

The SOLRAD 9 satellite also carries two additional telemetry systems, both PCM. One transmits continuously the data being stored in the memory system, while the other transmits the data that have been stored in the memory on command from a ground station. All data that are stored are also transmitted in real time by the FM/AM system.

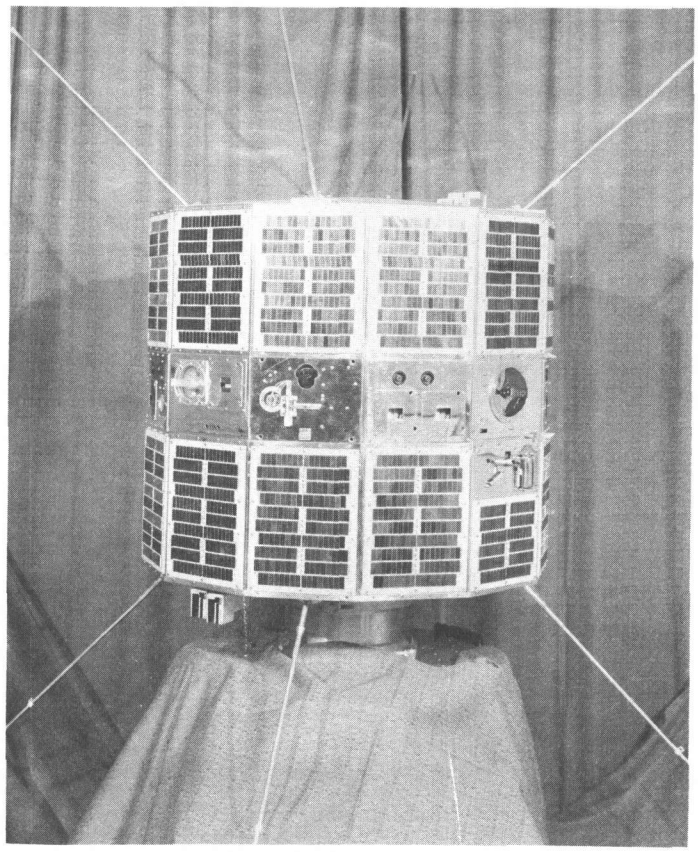

Fig. 1a - The SOLRAD 9 spacecraft. It is about 30 in. in diameter. Each of the 12 faces is covered with solar cells except in the central portion, where the x-ray photometers are mounted. The large circular device right of center is the aspect sensor. Below it are the nozzles for the spin attitude-control system. On the top and bottom of the spacecraft are located the antennae and the solar sensors of the attitude-control system.

Individual scientists and institutions have been invited through COSPAR to receive and use the x-ray data in their own programs of research. It is the purpose of this report to provide all information necessary for the reduction of the satellite data transmitted in real time. For satellite-tracking purposes, the orbital elements and equator crossings are available as bulletins from the NASA Computing Center at Goddard Space Flight Center.*

Information concerning the experiment and spacecraft status will be published in the Spacewarn Bulletin by IUWDS World Warning Agency, Box 178, Fort Belvoir, Virginia, U.S.A. 22060.

*Arrangements for being placed on the mailing list for these bulletins should be made through the Director, Naval Research Laboratory, Washington, D.C. 20390, Attention Code 7125.

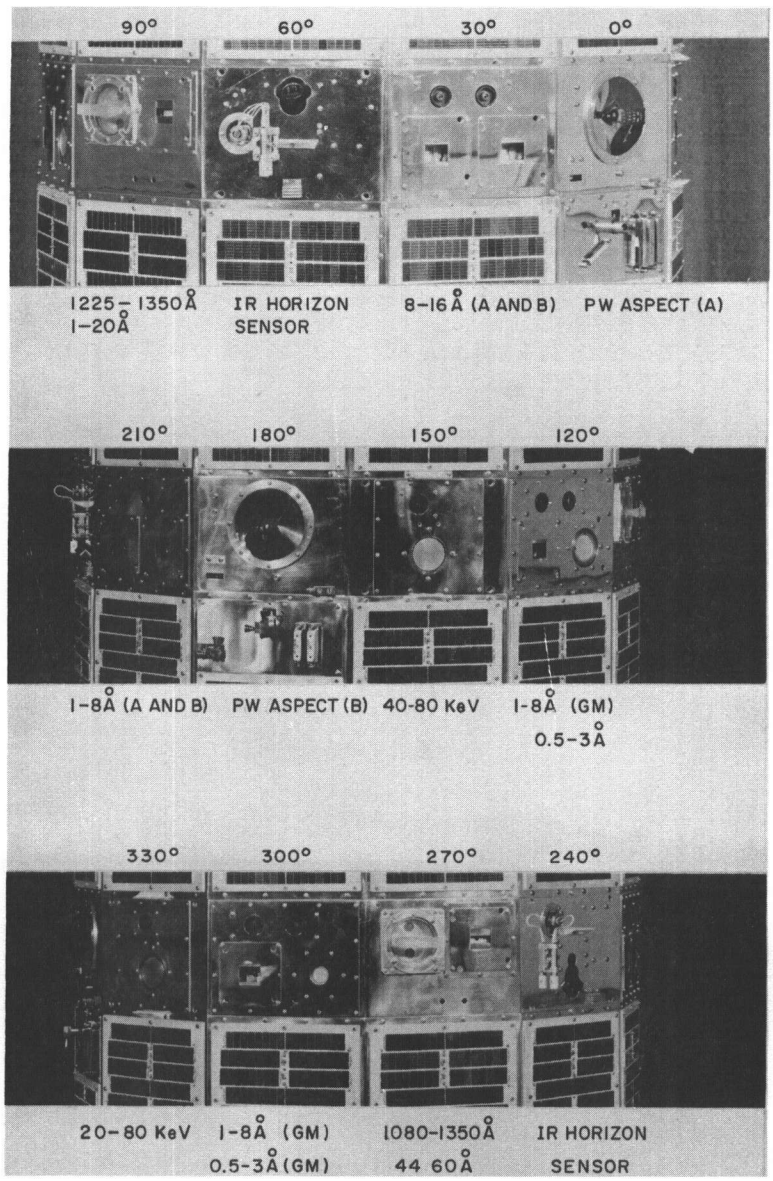


Fig. 1b - Three views of the spacecraft, taken at about 120-degree intervals. In this figure the location of each face is designated by its roll angle relative to the pulse-width aspect sensor A. See Table 1 for a complete description of each of the photometers.

## THE EXPERIMENTS

The design of the SOLRAD 9 experiments is based on experience gained from the reduction of SOLRAD 8 (Explorer 30) data as well as on the anticipated increase of activity in the solar cycle. As activity increases on the sun, we may expect that wide variations will occur in x-ray emission. There will be large changes between periods of relatively low sunspot activity and high activity. There will also be many more flare events, causing extremely large transient bursts of x-ray radiation of high energy. All of these effects have been anticipated in the design of the experiments.

The experiments are designed to measure radiation in the x-ray bands 44 to 60 Å, 1 to 20 Å, 8 to 16 Å, 1 to 8Å, and 0.5 to 3 Å, and from 20 to 80 kev. Two ultraviolet bands were also to be measured: 1080 to 1350 Å, and 1225 to 1350 Å.

The detectors are the standardized ionization chambers similar to those flown in SOLRAD 8. Their wavelength or energy response curves are illustrated in Figs. 2 through 7, and Table 1 contains all of the information required to calculate the wavelength responses of the photometers.

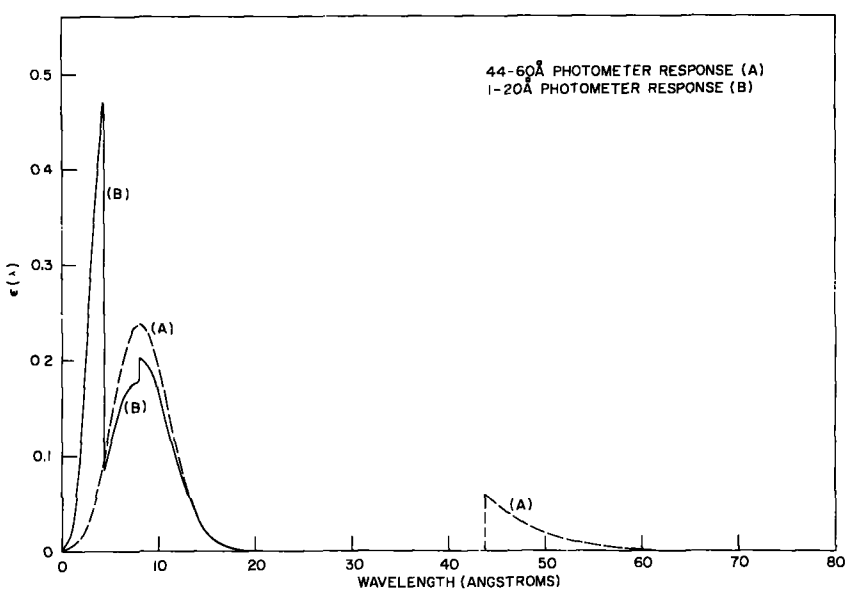


Fig. 2 - Wavelength response curves for the 44 to 60 Å (A) and the 1 to 20 Å (B) ionization chamber photometers

Because of the increase in solar activity, the dynamic range of each of the experiments has been reevaluated. Adjustments of amplifier sensitivity and photometer window area have been made to insure that "on-scale" measurements may be made in all solar-flare events, at least with the detectors devoted to the hardest radiation. Figure 8 illustrates the dynamic ranges of the 0.5 to 3 Å, 1 to 8 Å, 8 to 16 Å, and 44 to 60 Å photometer amplifier combinations of SOLRAD 9.

As with SOLRAD 8, broom magnets have been installed in front of the soft x-ray photometers to protect them from charged particles of the Van Allen belts. The effectiveness

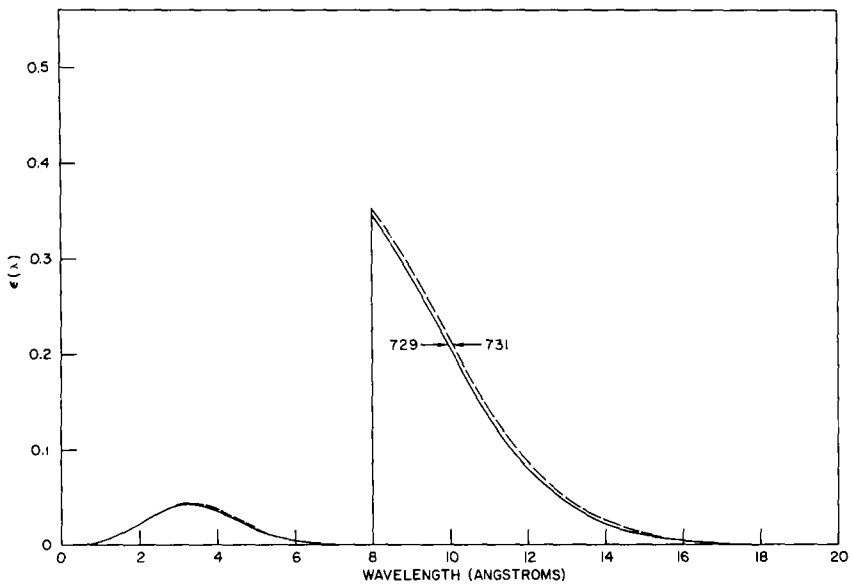


Fig. 3 - Wavelength reponse curves for the primary (731) and secondary (729) 8 to 16 Å ionization chamber photometers

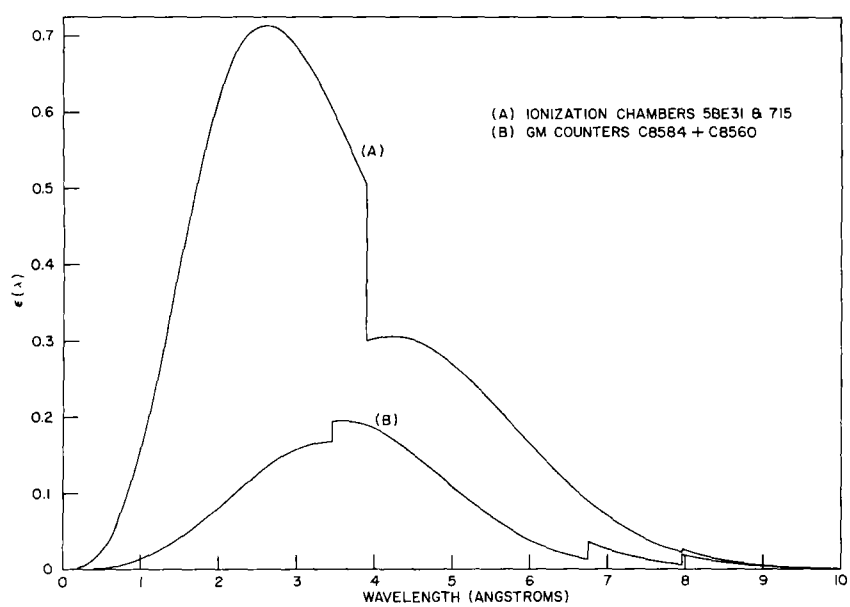


Fig. 4 - Wavelength response curves for the 1 to 8 Å detectors. The response of the ionization chamber photometers 5BE31 and 715 is indicated by curve A and that for the Geiger counter photometers C8584 and C8560 by curve B.

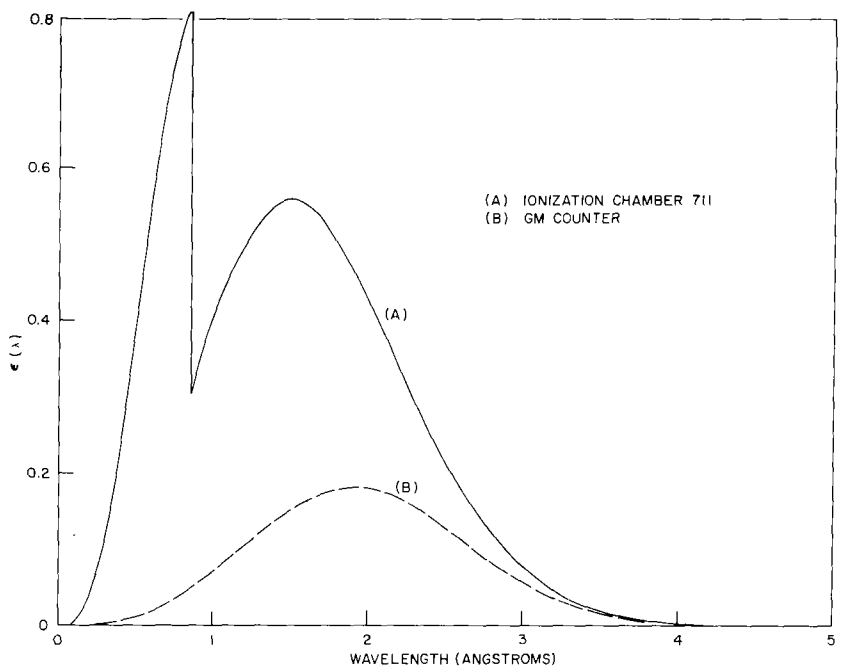


Fig. 5 - Wavelength response curves for the 0.5 to 3 Å experiments. The curve labeled A is the ionization chamber photometer 711, and that marked B is for the Geiger counter covering this region.

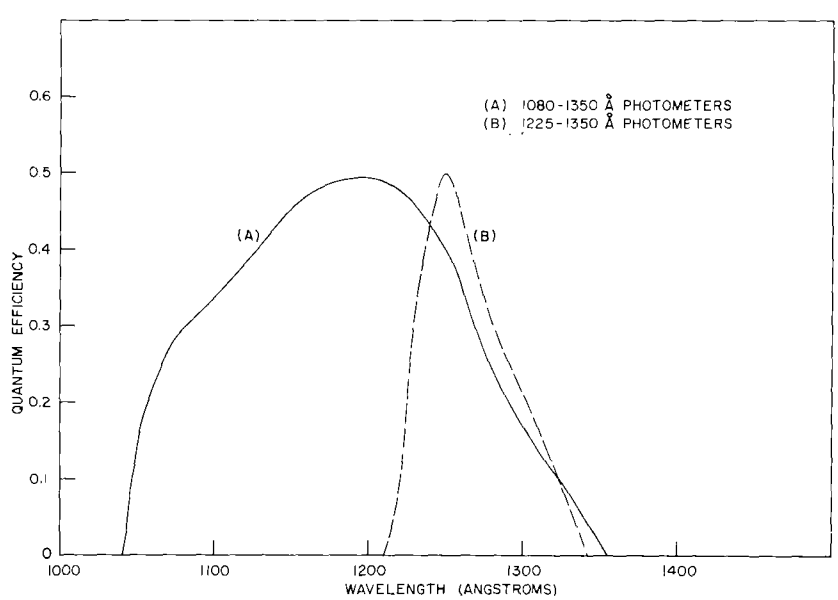


Fig. 6 - Quantum efficiency of the SOLRAD 9 ultraviolet photometers. The curve labeled A is the response of the 1080 to 1350 Å photometer, and that marked B is the response of the 1225 to 1350 Å photometer.

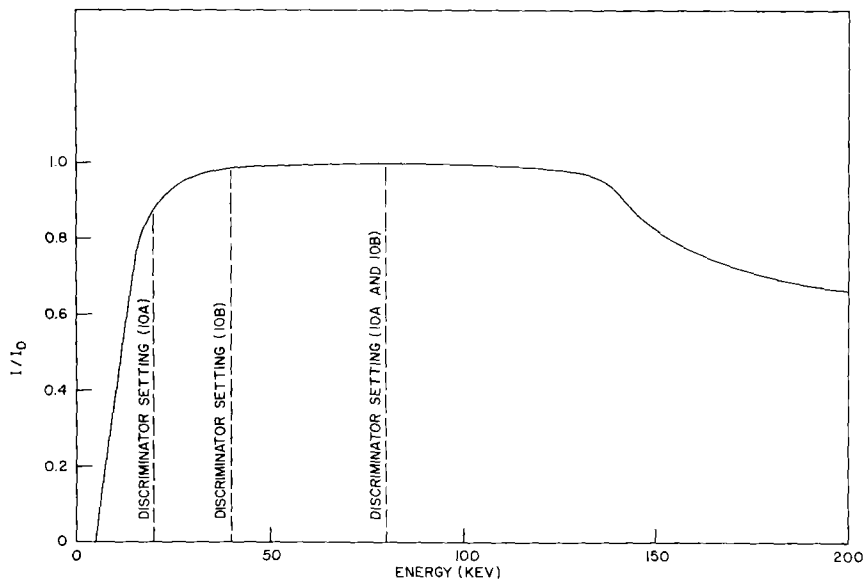


Fig. 7 - Relative efficiency as a function of x-ray energy in kev for the scintillation counter detector. The regions of interest, 40 to 80 kev and 20 to 80 kev, are determined by pulse-height discriminators. Designations 10A and 10B refer to experiment numbers.

of these magnets in eliminating response to electrons of energy less than 1 Mev was demonstrated by flying a photometer with a dummy magnet in 1965-16D, SOLRAD 7B. To reduce possible bremsstrahlung produced in the magnet pole faces, they are covered by beryllium shims 0.015 in. thick.

## SPACECRAFT DESCRIPTION

The spacecraft is a 12-sided drum about 30 in. in diameter and 30 in. long (Fig. 1). Internally the structure consists of a load-bearing tube about 8 in. in diameter which connects the mounting flange to a honeycomb structure which is the main support member for the electronic and mechanical components. An equatorial band about 8 in. high is located at the outer edge of the homeycomb platform. In this band are mounted the x-ray and ultraviolet photometers. As the satellite spins, the photometers view the sun for a short period once per revolution if the angle between the equatorial plane (perpendicular to the spin axis) and the direction to the sun is sufficiently small.

Above and below the equatorial band are mounted 24 solar-cell panels, each 7 by 10 in., covering the vertical surfaces. The battery pack is pressurized and mounted within the central tubular support structure. Two folding turnstile antenna systems project at 45-degree angles from the top and bottom of the payload. All structural support members, the equatorial band, and the top and bottom of the payload are covered with coatings providing thermal control.

The SOLRAD 9 satellite carries an attitude-control system and a spin-replenishment system similar in principle to those flown in SOLRAD 8. It is the purpose of these devices to maintain the satellite spin rate at a nominal 1 rps and the aspect angle to within

Table 1
SOLRAD 9 Flight Photometers

| Experiment | Position: Experiment No. | Position: Deg* | Det. No. | Window Matl. and Thickness† (cm) | $\rho x$ (W) (gm/cm$^2$) | Gas Filling and Pressure‡ | | Gas Filter Thickness§ | $\rho x$ (GW) (gm/cm$^2$) | $\rho x$ (G) (gm/cm$^2$) | $\omega$ (ion pair/erg) | Effective Window Area (cm$^2$)‡‡ |
|---|---|---|---|---|---|---|---|---|---|---|---|---|
| 8 - 16 Å Primary | 5A | 30 | 731 | Aluminum $8.9 \times 10^{-4}$ | $2.36 \times 10^{-3}$ | $N_2$ | 400 | 0.216 | $1.42 \times 10^{-4}$ | $1.67 \times 10^{-3}$¶ | $1.80 \times 10^{10}$ | 0.78 |
| 8 - 16 Å Secondary | 5B | 30 | 729 | Aluminum $8.9 \times 10^{-4}$ | $2.44 \times 10^{-3}$ | $N_2$ | 400 | 0.216 | $1.42 \times 10^{-4}$ | $1.67 \times 10^{-3}$¶ | $1.80 \times 10^{10}$ | 0.78 |
| 1 - 20 Å | 2 | 90 | 732 | Mylar $6.3 \times 10^{-4}$ Aluminum† $3.8 \times 10^{-5}$ | $8.5 \times 10^{-4}$ | $CCl_4$ | 27 | 0.216 | $5.27 \times 10^{-5}$ | $6.19 \times 10^{-4}$¶ | $2.13 \times 10^{10}$ | 0.174 |
| 44 - 60 Å | 1 | 270 | 745 | Mylar $6.3 \times 10^{-4}$ | $8.0 \times 10^{-4}$ | $N_2$ | 170 | 0.216 | $6.04 \times 10^{-5}$ | $7.10 \times 10^{-4}$¶ | $1.80 \times 10^{10}$ | 0.174 |
| 1225 - 1350 Å | 4 | 90 | 530 537 | Calcium Fluoride 0.2 | - | NO | 20 | - | Quantum Eff. 21% Quantum Eff. 21% | AV. 21% @ 1300Å | | $4.4 \times 10^{-2}$§§ |
| 1080 - 1350 Å | 3 | 270 | 1989 1981 | Lithium Fluoride 0.2 | - | NO | 20 | - | Quantum Eff. 50% Quantum Eff. 46% | AV. 48% @ 1216Å | | $1.9 \times 10^{-2}$§§ |
| 0.5 - 3 A IC | 7B | 120 | 711 | Beryllium 0.127 | 0.25 | Kr | 1520 | 0.094 | $7.0 \times 10^{-4}$ | $1.89 \times 10^{-2}$¶ | $2.57 \times 10^{10}$ | 5.28 |
| 1 - 8 Å GC | 8B | 120 | C8560 | Mica Beryllium 0.0076 | 0.00175 0.015 | Ne Br | 430 1% | - | - | $1.97 \times 10^{-3}$** | - | 0.32 |
| 1 - 8 Å GC | 8A | 300 | C8548 | Mica Beryllium 0.0076 | 0.00175 0.015 | Ne Br | 430 1% | - | - | $1.97 \times 10^{-3}$** | - | 0.32 |
| 40 - 80 kev | 10B | 150 | 743 | Aluminum 0.0127 | $3.43 \times 10^{-2}$ | NaI (Tl) Scintillator 3.6 cm dia. × 1 cm Thick RCA C 7151S PM | | | - | 3.67†† | - | 10.2 |
| 20 - 80 kev | 10A | 330 | 744 | Aluminum 0.0127 | $3.43 \times 10^{-2}$ | NaI (Tl) Scintillator 3.6 cm dia. × 1 cm Thick RCA C 7151S PM | | | - | 3.67†† | - | 10.2 |
| 1 - 8 Å IC Primary | 6A | 210 | 715 | Beryllium 0.0127 | $2.38 \times 10^{-2}$ | Ar | 760 | 0.094 | $1.7 \times 10^{-4}$ | $4.52 \times 10^{-3}$¶ | $2.38 \times 10^{10}$ | 1.18 |
| 1 - 8 Å IC Secondary | 6B | 210 | 5BE31 | Beryllium 0.0127 | $2.39 \times 10^{-2}$ | Ar | 760 | 0.094 | $1.7 \times 10^{-4}$ | $4.52 \times 10^{-3}$¶ | $2.38 \times 10^{10}$ | 1.18 |
| 0.5 - 3 Å GC | 7A | 300 | - | Mica Beryllium 0.127 | 0.00175 0.25 | Ar Br | 225 1% | - | - | $2.05 \times 10^{-3}$** | - | 2.43 |

*Measured in degrees from face 1 in direction of rotation
†Overcoating of evaporated aluminum 1500 Å
‡Pressure in mm corrected to 0° C
§Distance between window and internal grid in cm
¶Depth of sensitive volume of ionization chambers 2.54 cm
**Depth of sensitive volume of Geiger Counters 3.87 cm
††Surface density of NaI (Tl) crystal in gm/cm$^2$
‡‡cm$^2$; Attenuation factors have been included in area calculation
§§Area for both photometers

± 1 degree of the direction to the sun. The attitude-control system consists of a toroidal tank containing 11 lb of liquid ammonia which is allowed to pass through two sets of solenoid valves to two redundant nozzles. The solenoid valves are controlled by solar sensors located 90 degrees away from the nozzles and the equatorial band of the satellite. The spin-replenishment system consists of a smaller toroidal tank containing two pounds of liquid ammonia. The valve arrangement is similar to that used with the attitude-control system, but the valves are controlled by radio command. The pressure in both tanks will vary between 50 and 375 psi, depending on the tank temperature. A backup spin-replenishment system uses a cylindrical tank containing 0.5 lb of ammonia. The valve arrangement is made up of two solenoid valves in series to provide insurance against leakage and buildup of spin rate.

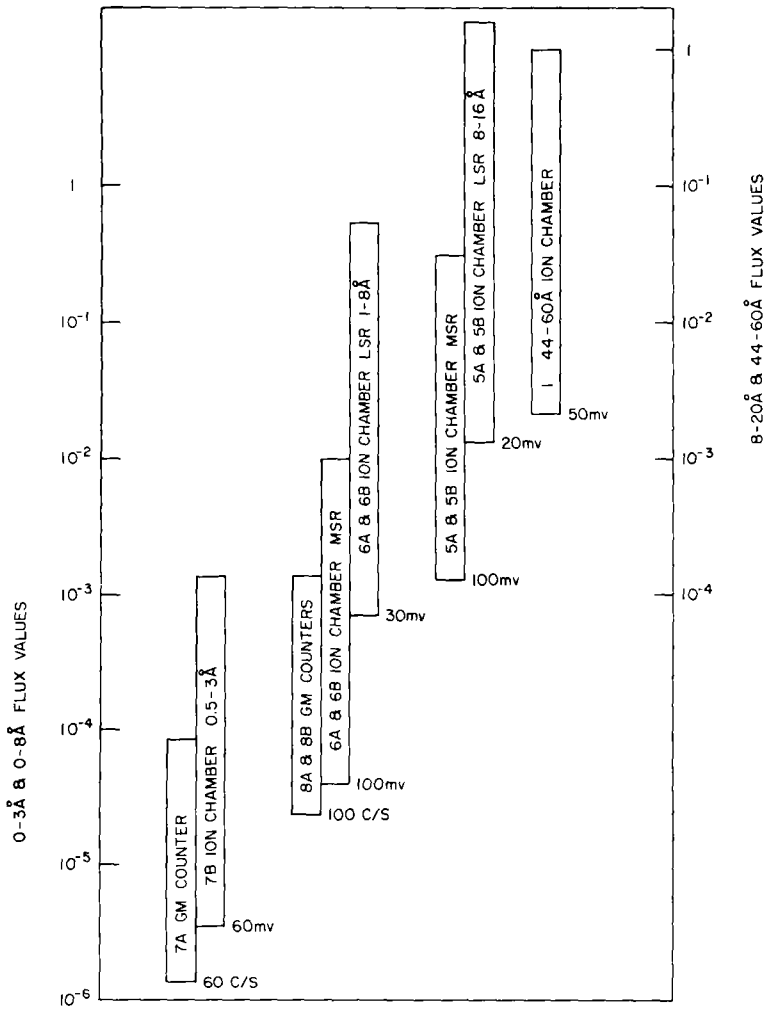


Fig. 8 - Graphic description of the dynamic range of the SOLRAD 9 x-ray experiments. The maximum levels are determined by the inability of the subcarrier oscillators to transmit a signal greater than 5 volts without distortion. The minimum levels are determined by the noise level of the electrometer amplifier and by the window area of the photometer.

Three telemetry systems are used in the satellite. The primary system for real-time data transmission is an FM/AM system radiating on 136.53 MHz with a power output of 150 milliwatts. This system consists of six voltage-controlled subcarrier oscillators, IRIG channels 3 through 8, which are frequency modulated by the inputs from the experiment electronic circuits. The voltage-controlled subcarrier oscillator outputs are linearly mixed and amplitude modulate the rf carrier. A 32-segment commutator on IRIG channel 3 contains "housekeeping" information, channels 4 through 7 contain x-ray and ultraviolet data, and channel 8 contains solar-aspect data.

The secondary telemetry system is also an FM/AM system, but radiates on 137.59 MHz with a power output of 150 milliwatts. This system consists of four voltage-controlled oscillators, IRIG channels 3, 6, 7, and 12, which are frequency modulated by

their individual inputs. A 32-segment commutator on IRIG channel 3 contains additional "housekeeping" information, IRIG channels 6 and 7 are used for earth albedo measurements, and channel 12 is used for PCM telemetry data.

The third system has a PCM system radiating on 137.41 MHz with a power output of 500 milliwatts (cw). This system is used for the transmission of data stored from three x-ray photometers in a 54-kilobit core memory. This memory is read out by ground command.

Two command receivers and two decoders drive a matrix which has 48 outputs. These outputs are used to operate the experiments in different modes, turn all or part of the payload on or off, activate ordnance devices, replenish spin, etc. The command receivers share the top turnstile antenna system with the primary telemetry system.

A clock has been provided which feeds a register one pulse every four minutes. The register is read out nondestructively into the memory at the beginning of a recording sequence. Once every four minutes the register output is placed on IRIG channel 5 of the primary data-transmission system.

## DESCRIPTION OF THE SOLRAD 9 EXPERIMENTS

### The Aspect System

The aspect sensors measure the angle between the satellite equatorial plane and the direction to the sun. Although the satellite spin axis is oriented to be perpendicular to the solar vector to within $\pm 5°$, the aspect sensors have been included to measure the performance of the attitude-control system and to provide aspect-angle measurement in case of a malfunction of that system. Since all data reduction depends on the precise determination of aspect angle, two sensors have been included which are completely redundant. The primary sensor is on the 0-degree face, and the secondary sensor is located 180 degrees from it, on the opposite face (Fig. 1a). Either sensor can be selected by ground command. Unless there is a malfunction, the primary sensor will always be used in order to simplify routine data reduction.

The sensors themselves are quite similar to those flown on SOLRAD 8.* A solar cell located at the apex of a cone views the sun once per satellite rotation. Two circular masks, each one half the cone diameter, chop the light in such a way that two pulses are formed at the output of the amplifier. The aspect angle can be derived from the width and spacing of these pulses.

In the center of the aspect sensor, at the point of intersection of the two circular masks, a grey code reticle has been mounted. This reticle provides a "digital" readout of the solar-aspect angle for angles smaller than $\pm 6$ degrees. The reticle design has been improved over that used in SOLRAD 8 to increase its resolution.

Figure 9 is a photograph of the aspect reticle, and in Fig. 10 a diagram from which the aspect angle can be calculated for angles between -6 and +6 degrees is presented. In Fig. 11, a sample record showing the actual appearance of the aspect signal has been reproduced. To obtain the value of the aspect angle, one simply reads the pattern of pulses between the two large pulses in the direction of increasing time (right to left) as illustrated in Fig. 11. The angle can then be obtained by matching the pulse pattern with the reticle pattern in Fig. 10.

---

*"Final Data and Calibrations for the Explorer 30 (NRL SOLRAD 8) X-Ray Monitoring Experiment," unpublished NRL report.

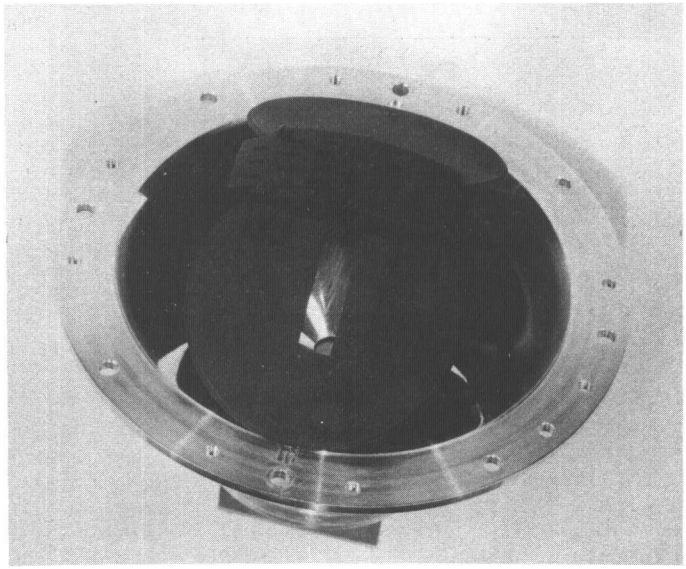

Fig. 9 - The solar-aspect sensor, showing the gray-code reticle designed to produce a digital readout of aspect angles between plus and minus six degrees. The direction of rotation of the unit is along the longer dimension of the gray-code reticle.

For angles larger than +6 and -6 degrees, another technique will have to be used for reduction of the aspect angle. Although the attitude-control system is expected to hold the aspect angle within ±6 degrees, information pertaining to the pulse-width aspect system is included here in case of a malfunction of the spin-axis attitude-control system. The pulse-width ratio is defined in Fig. 12, where an expanded tracing of an individual aspect pulse from a SOLRAD 8 telemetry record has been reproduced. Once the pulse-width ratio has been measured from a record, the aspect angle can be determined from the calibration curves in Figs. 13 and 14.

## Primary 1 to 8 Å X-Ray Photometer Experiment

The 1 to 8 Å ion-chamber photometer experiment, which together with the 8 to 16 Å experiment are considered the primary experiments, is assigned IRIG telemetry channel 4 to insure uninterrupted coverage of x-ray flare events. The signals from this photometer are also read and stored once each minute in the spacecraft data-storage system. The stored data are read out twice per day by the NRL ground station at Blossom Point, Maryland. Because of the importance of this experiment, both the photometer and electrometer amplifier may be replaced by ground command. The photometer, which is in operation at any time, is indicated by subcommutator segment 25 on channel 3. The subcommutator will be described in detail later.

The electrometer amplifier used with this photometer has two sensitivity ranges, and it switches automatically from the most sensitive range (MSR) to the least sensitive range (LSR) when the output signal reaches 5 volts. To change back from the least sensitive to the most sensitive range requires that a pulse be received from the memory unit. This pulse is called the relative time advance pulse. The sensitivity status of the

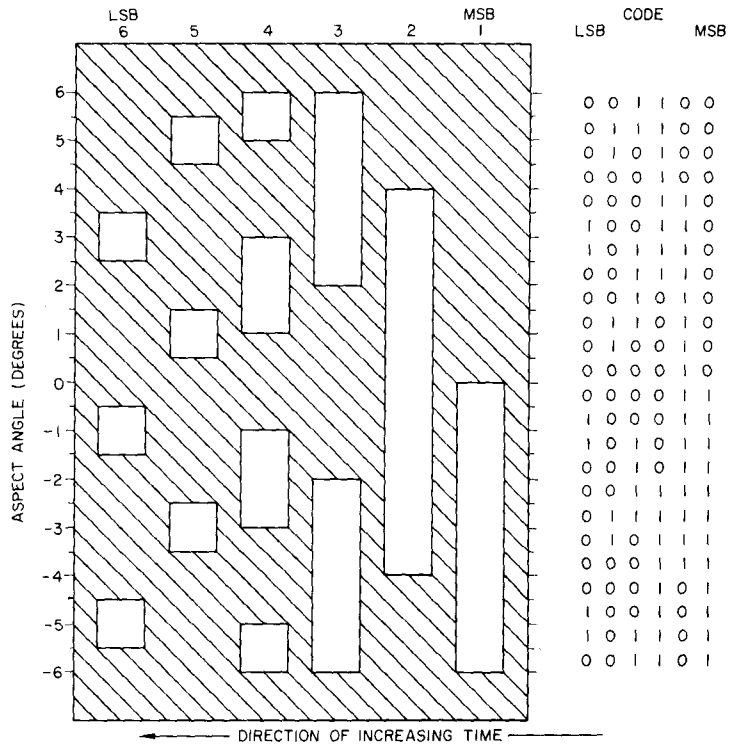


Fig. 10 - Schematic representation of the gray-code aspect reticle. The aspect angle can be read directly from this schematic by matching the ones and zeros in the telemetry recording with the corresponding pattern in the diagram.

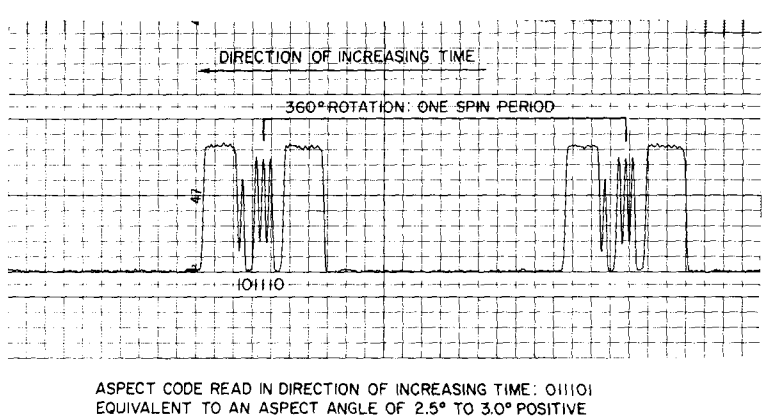


Fig. 11 - Reproduction of an actual telemetry signal, showing the gray-code pattern for an aspect angle of 2.5 to 3.0 degrees positive

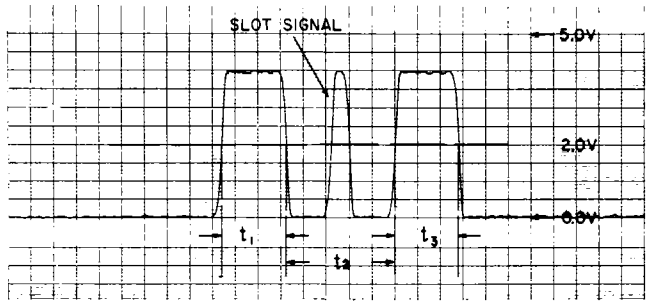


PULSE WIDTH RATIO; $PWR = \frac{2t_2}{t_1+t_3}$

SLOT SIGNAL IS PRESENT FOR NEGATIVE ASPECT ANGLES (SUN BELOW SATELLITE EQUATOR) BETWEEN 10° AND 40°

Fig. 12 - Reproduction of a telemetry recording of the pulse-width-aspect signal for an angle greater than ± 6 degrees.

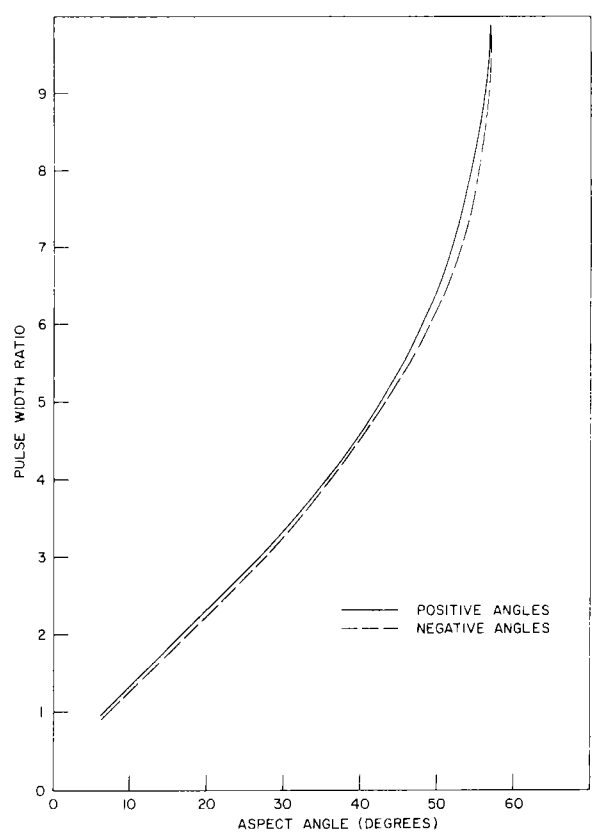


Fig. 13 - Calibration curve for pulse-width-aspect sensor 9B. The pulse width ratio is defined in the text and in Fig. 12.

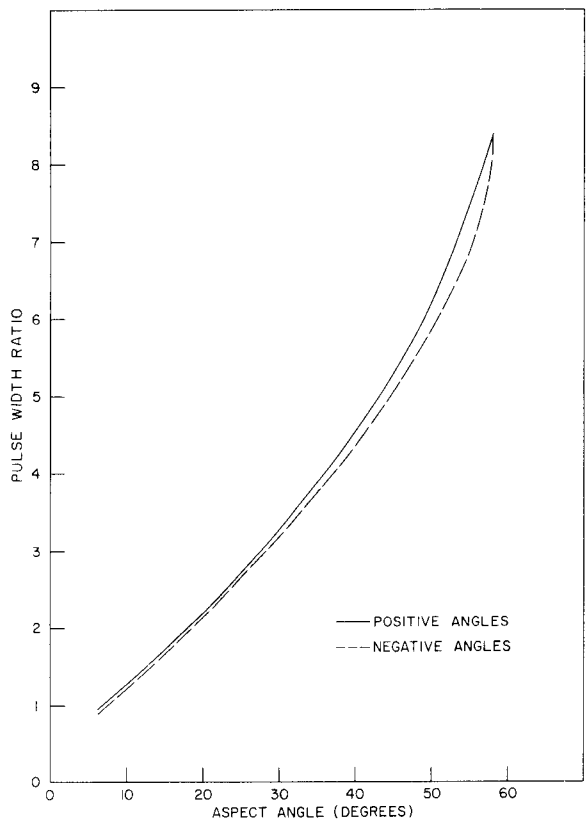


Fig. 14 - Calibration curve for pulse-width-aspect sensor 9A

1 to 8 Å experiment can be read from commutator segment 27 on IRIG channel 3. In case of a malfunction, it is possible to override the automatic range-change circuit and control the range selection manually. Commutator segment 26 indicates whether the experiment is in manual or automatic mode. Calibration curves for conversion of output voltage to input current for both ranges of the two electrometers are shown in Fig. 15.

In case of a malfunction of the attitude-control system, it will be necessary to make a correction to the 1 to 8 Å peak response for the aspect angle. For this purpose, the angular response of the 1 to 8 Å photometers is illustrated in Figs. 16 and 17.

## Primary 8 to 16 Å X-Ray Photometer Experiment

The 8 to 16 Å experiment is similar to the 1 to 8 Å experiment, in that a two-range amplifier is used, with one IRIG subcarrier channel (No. 5) exclusively devoted to the analog output of this experiment. The signals are sampled and stored once per minute in the spacecraft data-storage system, and either of two photometer-amplifier combinations may be chosen by ground command. Segment 22 of the subcommutator indicates which of the two is operating at any time, segment 24 indicates whether the experiment is in the high or low sensitivity range, and segment 23 tells whether or not the experiment is changing range automatically or manually. Calibration curves for conversion of output voltage to input current for both ranges of the two electrometer amplifiers are shown in Fig. 18. If corrections for aspect angle are required, the angular-response curves in Figs. 19 and 20 may be used.

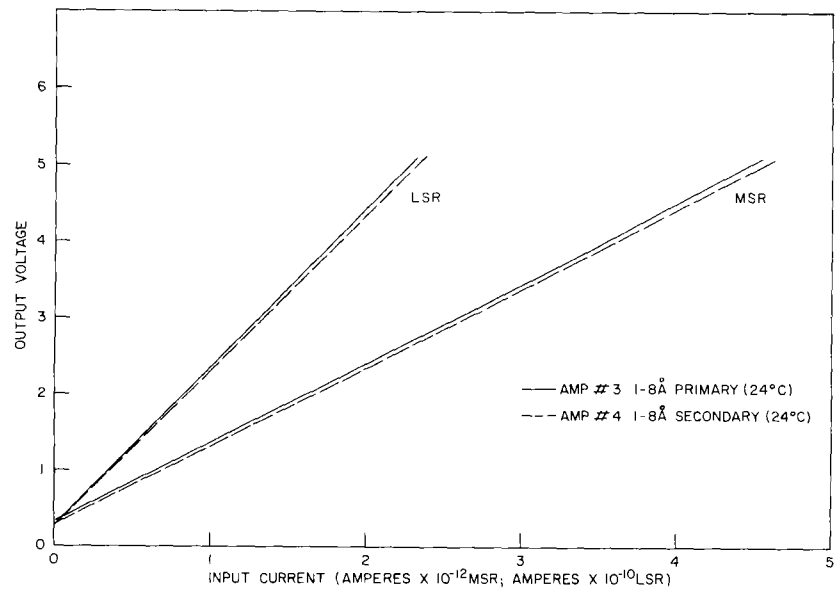


Fig. 15 - Current-to-voltage calibration curve for the electrometer amplifiers used with the 1 to 8 Å ionization-chamber photometers. These are a dual-range amplifiers. LSR indicates the calibration curves for the least sensitive range and MSR for the most sensitive range.

To provide a means of reading absolute time into the spacecraft data-storage system and to place on each real-time recording of the analog telemetry a unique identification, a 16-bit counter is read out every four minutes onto IRIG channel 5. This counter readout takes the place of the 8 to 16 Å photometer data, which normally appear on this channel. In Fig. 21 a portion of a telemetry record has been reproduced which shows the clock readout. The readout sequence is repeated four times. The bits are identified in Fig. 21 for only the second sequence. The NRZ binary number is read as follows:

| Bit No. | Binary N | Decimal |
|---|---|---|
| 1 | 1 | 1 |
| 2 | 0 | - |
| 3 | 1 | 4 |
| 4 | 1 | 8 |
| 5 | 1 | 16 |
| 6 | 1 | 32 |
| 7 | 1 | 64 |
| 8 | 1 | 128 |
| 9 | 0 | - |
| 10 | 1 | 512 |
| 11 | 1 | 1,024 |
| 12 | 0 | - |
| 13 | 1 | 4,096 |
| 14 | 1 | 8,192 |
| 15 | 1 | 16,384 |
| 16 | 0 | - |
| | | 30,461 |

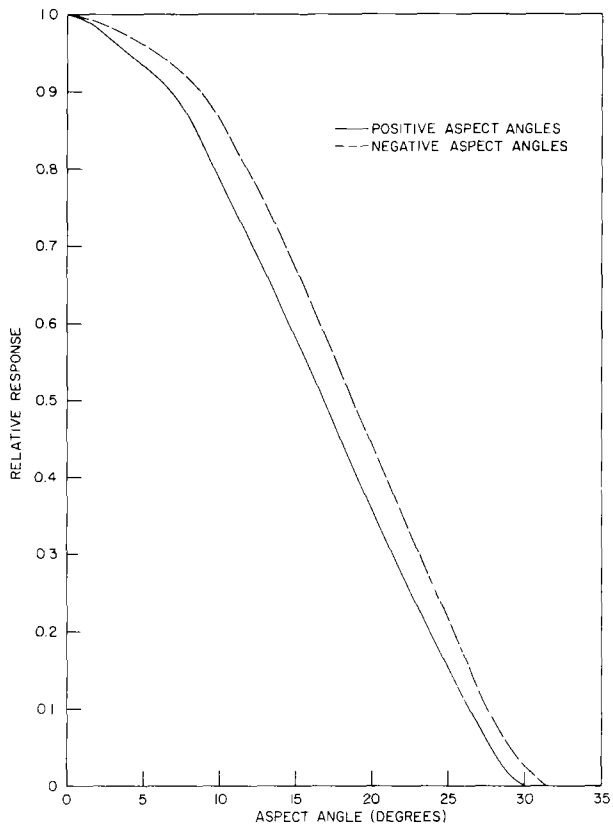


Fig. 16 - Angular response curve for the primary 1 to 8 Å photometer (715). A systematic error is present in the measurement of positive and negative angles. If one subtracts 1.5 degrees from the measured positive aspect angles and adds 1.5 degrees to the negative angles before using this correction curve, the error may be removed.

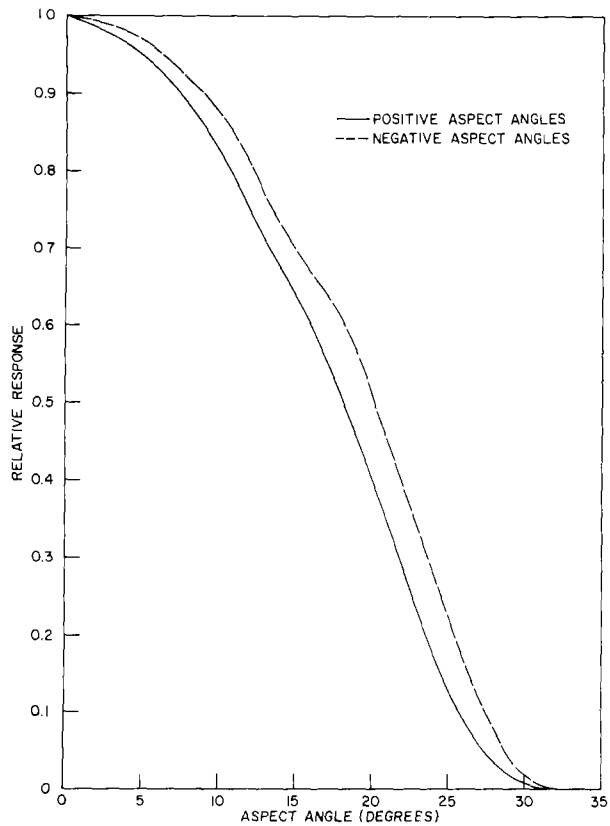


Fig. 17 - Angular response curve for the secondary 1 to 8 Å photometer (5BE31). See Fig. 16 caption.

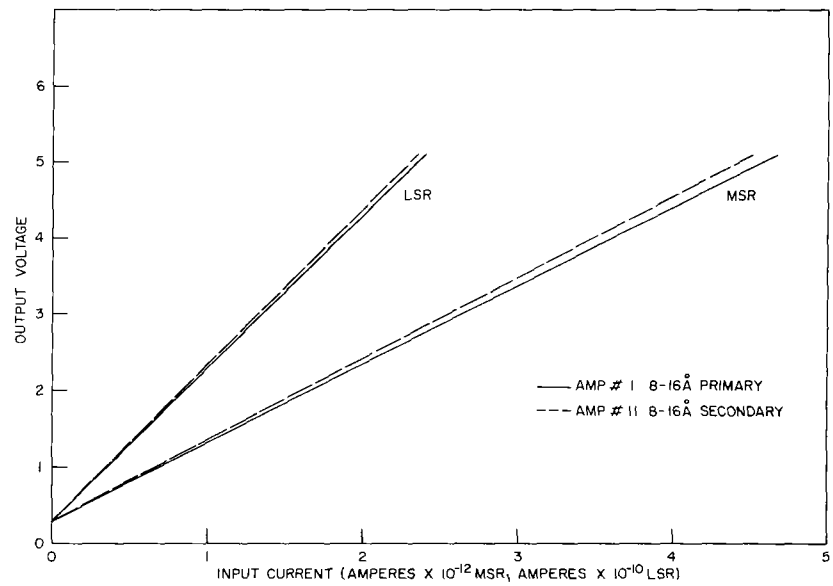


Fig. 18 - Current-to-voltage calibration for the electrometer amplifiers used with the 8 to 16 Å photometers

Note that to identify the beginning of a sequence, the least significant bit is separated into two parts. The first half of the bit has a level 95 percent of full scale and is always present whether the first bit is either a one or a zero. The second half of the bit is 78 percent of full scale and is not present if the first bit represents a zero. Note also that the first sequence is always one count less than the following three sequences.

As mentioned above, the counter is incremented once each four minutes. The total capacity of the counter is 65,535 counts, or about 181 days. After this time the counter will overflow and begin again to count at zero.

The counter becomes an indicator of absolute time by comparison of the count with some time standard such as WWV or a ground-station time-code generator.

## 0.5 to 3 Å Ion Chamber and Geiger Counter Experiments

The primary 0.5 to 3 Å experiment is an ionization chamber operating into a single-range electrometer amplifier. The signals from this photometer are also sampled by the spacecraft data-storage system once per minute to obtain the time history of flare emission.

In an attempt to measure the level of solar x-ray radiation below 3 Å during quiet periods, a Geiger counter was installed which had about two times the sensitivity of the ion-chamber experiment. The signals from this experiment are expected to be saturated during solar flares, and so it was not considered of importance to store the data from this experiment.

The calibration curves for these two experiments are given in Figs. 22 and 23, and their angular response curves appear in Figs. 24 and 25.

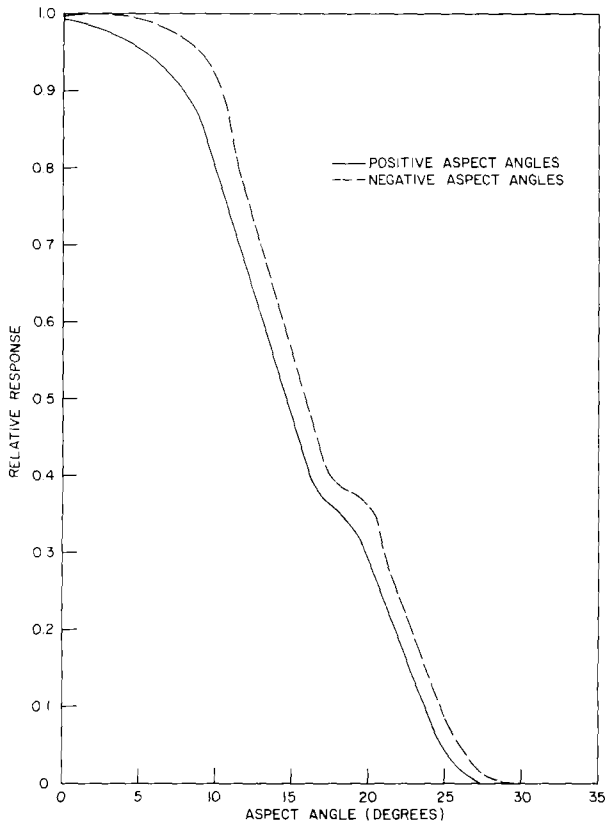


Fig. 19 - Angular response curve for the primary 8 to 16 Å ionization chamber photometer (731). See Fig. 16 caption.

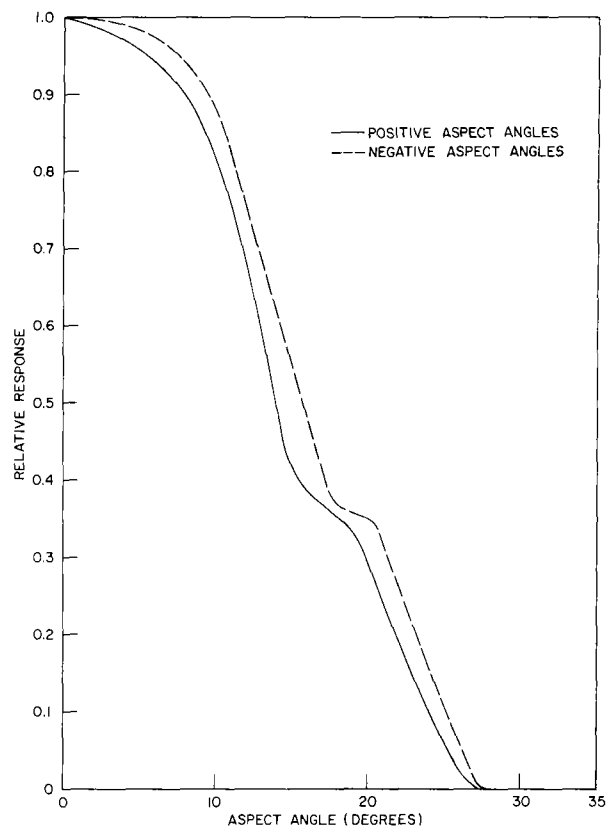


Fig. 20 - Angular response curve for the secondary 8 to 16 Å ionization chamber photometer (729). See Fig. 16 caption.

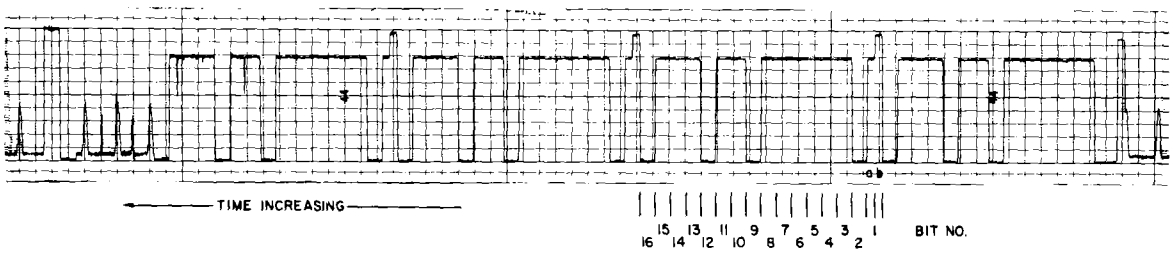


Fig. 21 - Reproduction of a section of telemetry record from IRIG channel 5, showing the spacecraft clock readout. See text for a description of this readout.

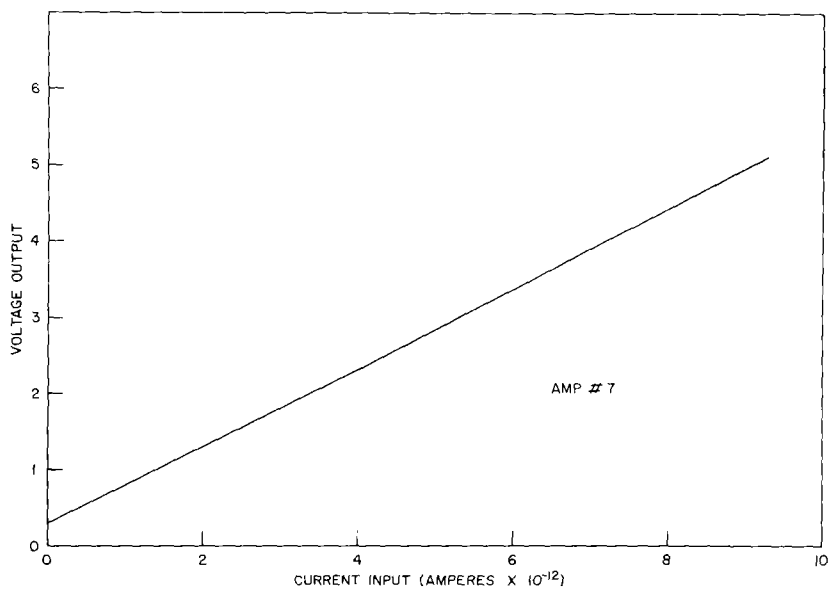


Fig. 22 - Voltage-current calibration for the 0.5 to 3 Å electrometer amplifier

The signals from these two experiments appear on IRIG channel 6, together with the 1 to 8 Å Geiger counter and the scintillator experiment outputs. The data format will be described later.

## 1 to 8 Å Geiger Counter Experiment

This experiment was included to make measurements of x-ray radiation below 8 Å during quiet periods. The data are not stored, because the signals are usually saturated during solar flares. At those times the 1 to 8 Å ionization-chamber experiment is operating on scale and providing data for storage in the memory system. Redundant detectors and ratemeters are provided which may be selected by ground command. Commutator segment 29 indicates which of the detectors is on at a particular time.

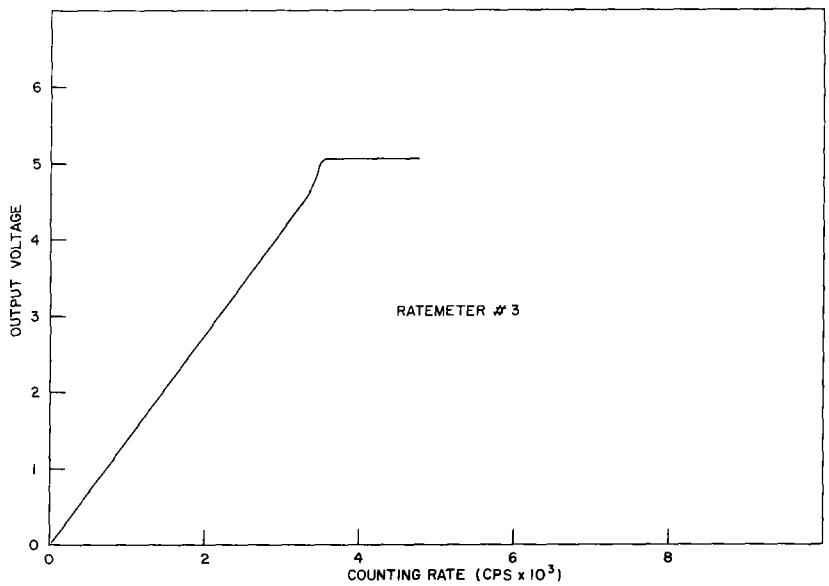


Fig. 23 - Voltage-counting-rate calibration curve for the rate meter used with the 0.5 to 3 Å Geiger counter photometer

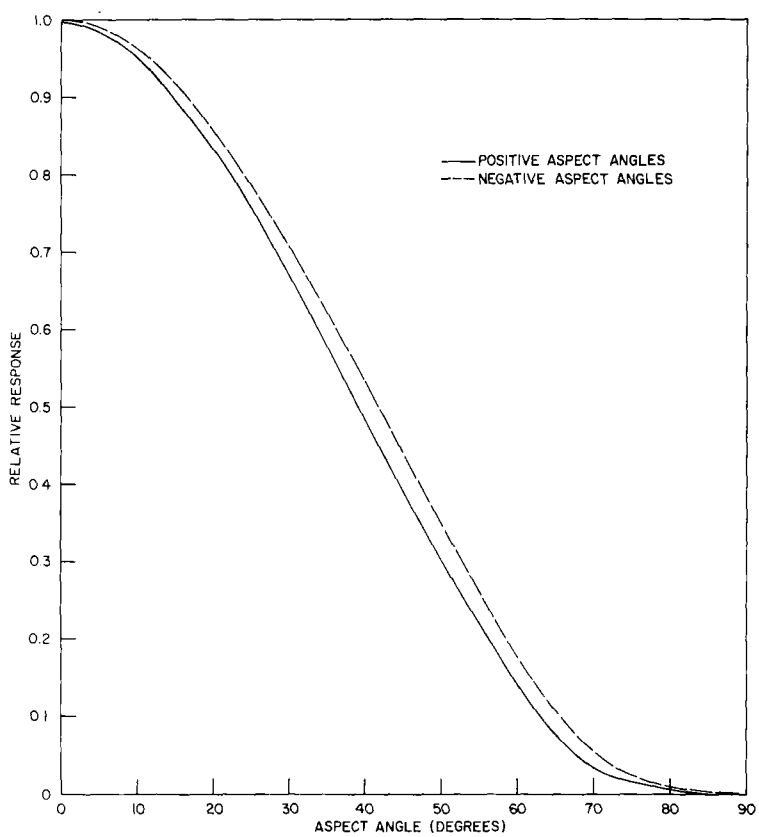


Fig. 24 - Angular response of the 0.5 to 3 Å ionization chamber photometer (711). See Fig. 16 caption.

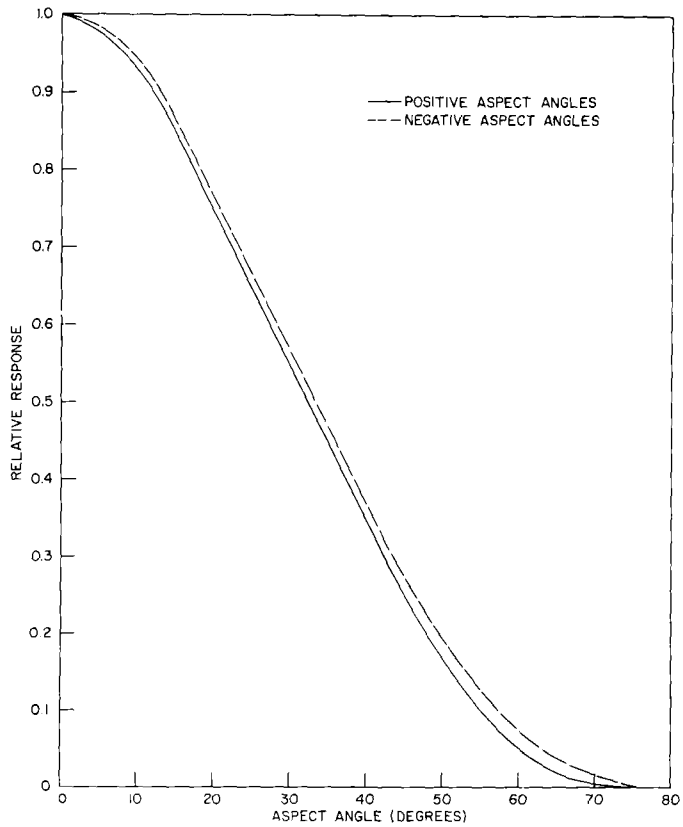


Fig. 25 - Angular response of the 0.5 to 3 Å Geiger counter photometer. See Fig. 16 caption.

Two high-voltage power supplies have been provided for this Geiger Counter experiment. These supplies have different voltages and may be changed by ground command to compensate for any changes of the counter operating voltage due to anticipated aging of the counter. The supplies may also be turned on or off by ground command. Segment 30 of the channel 3 commutator indicates the status of the 1 to 8 Å Geiger counter power supplies. The calibration and angular response curves for the 1 to 8 Å Geiger counter experiment are given in Figs. 26, 27 and 28.

### Scintillation Counter Experiment for Solar X-Rays 40 to 80 and 20 to 80 kev

Two scintillation counters were installed on opposite faces of the satellite together with solar eyes which have an acceptance angle of ±7 degrees in the roll direction. As the satellite spins, one of the solar eyes opens a gate which permits counts from the photomultiplier on that same face to be accumulated in a foreground register for the period when the experiment is viewing the sun. After a roll of 180 degrees the opposite eye views the sun. This eye opens another gate, permitting the counts from the scintillator to be accumulated in a background register. The total period for which counts are accumulated is determined by the 32-sec data frame employed in both IRIG channels 6 and 7. The fourth set of calibration signals (0.5 sec - 0 volts, 0.5 sec - 5.0 volts, which are not present in the analog readout) act to close the gates to the foreground

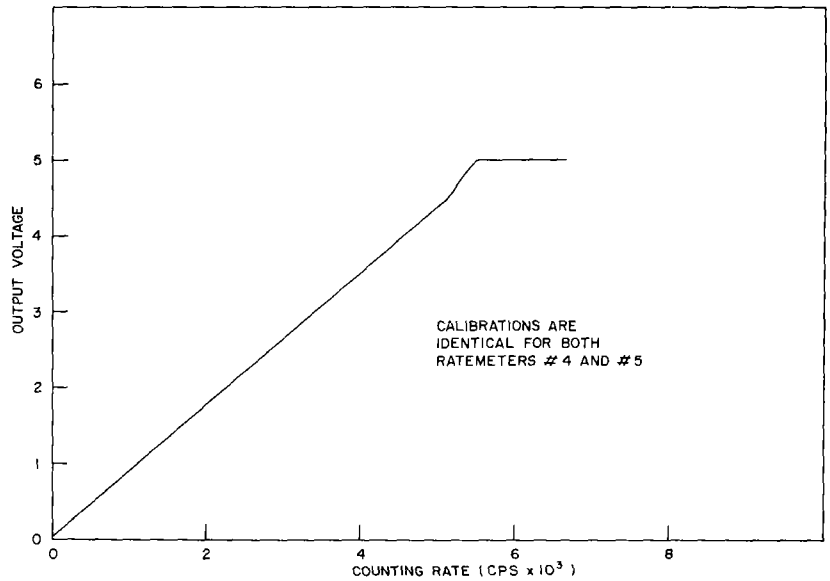


Fig. 26 - Voltage-counting-rate calibration curve for ratemeters used with the 1 to 8 Å Geiger counter photometers

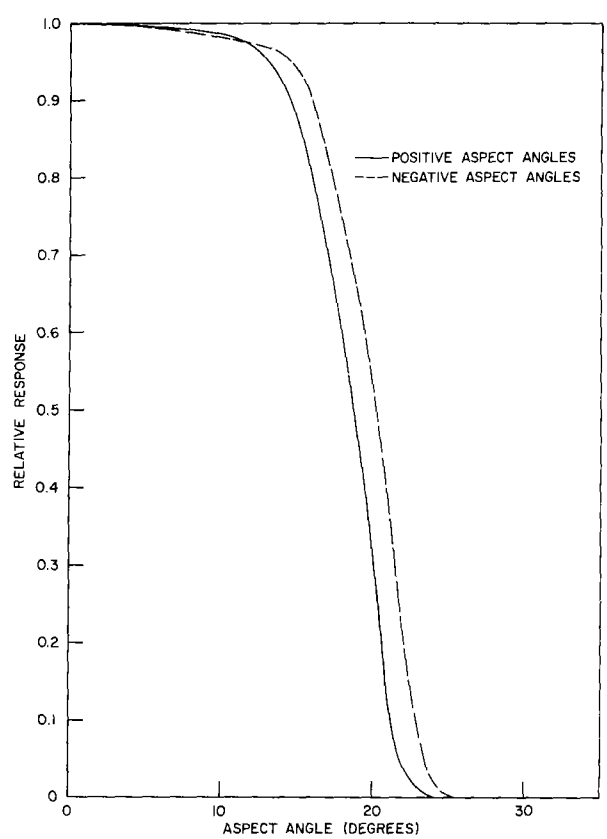


Fig. 27 - Angular response of 1 to 8 Å Geiger counter photometer (C8548). See Fig. 16 caption.

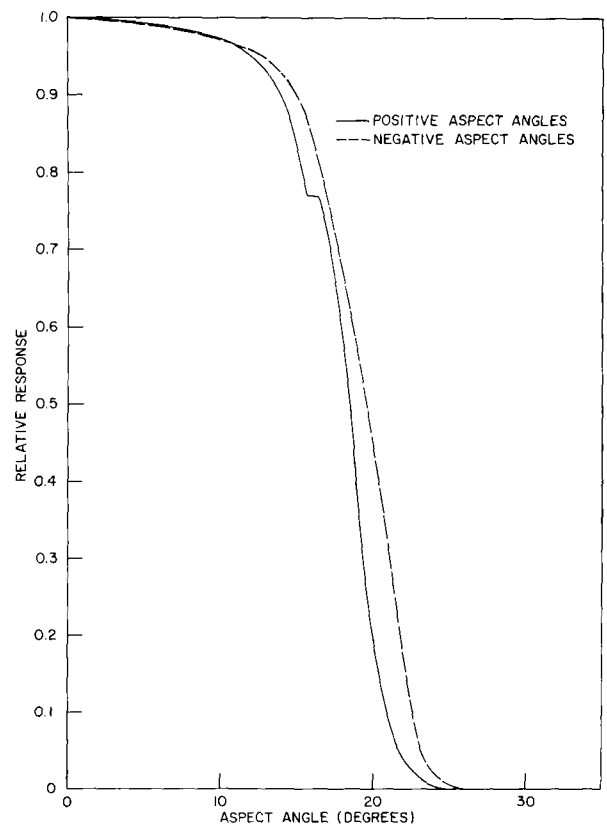


Fig. 28 - Angular response of 1 to 8 Å Geiger counter photometer (C8560). See Fig. 16 caption.

and background registers and permit them to be read out in the fourth subframe of the 32-sec data frame. This means that the total period over which counts are accumulated is 24 sec, and if the satellite is spinning at 1 rps, 24 samples of foreground counts will be summed in the foreground register, and 24 samples of background counts will be summed in the background register.

The foreground and background registers are read out in sequence in the fourth subframe of the channel 6 data frame. Each of the registers has ten bits and is read out in an NRZ code. This analog readout is illustrated in Fig. 29. The sequence in order of increasing time is as follows:

- 0.1 sec – flag pulse – 87 percent indicating beginning of readout.
- 2.7 sec – ten bits foreground data, NRZ code, MSB (512) first, 1 level is 60 percent and zero level is 0 percent of full scale.
- 2.9 sec – ten bits background data, NRZ code, MSB (512) first, LSB is wider than other bits.
- 1.3 sec – zero level

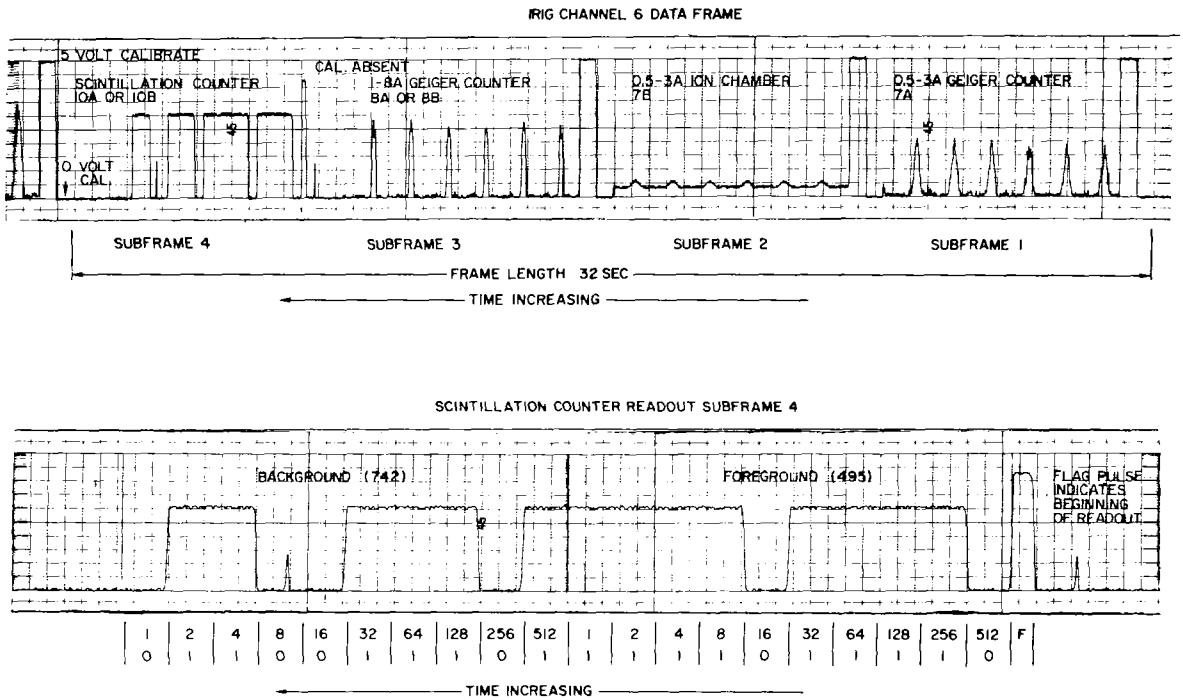


Fig. 29 - Readout of IRIG channel 6 data frame from telemetry record, and expanded scintillation counter readout from channel 6, subframe 4

The 40 to 80 or 20 to 80 kev scintillation counter may be selected by ground command or may be turned on or off. Segment 32 on channel 3 provides the necessary information to determine the experiment status.

Background counting rates have turned out to be much greater than expected, and no provision has been made to indicate overflow of either of the registers. A malfunction developed soon after launch in one of the trigger eyes. Apparently its sensitivity decreased, resulting in loss of the background data for one scintillator and the foreground data for the other scintillator. For these reasons no further effort has been made to develop calibrations and corrections for data reduction from this experiment.

## Ultraviolet Ionization Chamber Experiments

Two pairs of ionization chambers are included in the instrumentation of the SOLRAD 9 spacecraft to measure solar ultraviolet radiation in the wavelength ranges 1080 to 1350 Å and 1225 to 1350 Å. For each range, two ion chambers were connected in parallel so that a failure of one ion chamber would not mean a complete loss of data for that wavelength range. A set of screen grids was installed in front of each pair of photometers to repel electrons. The outer grid was held at a potential of -45 volts and the inner at +45 volts.

Two basic changes were made in the SOLRAD 9 ultraviolet experiments which made them unlike the SOLRAD 8 instruments. First the amplifier sensitivity was decreased and the window open area increased. It was hoped that with larger window areas it would be possible to provide better laboratory calibrations of the ion chambers. Because it is

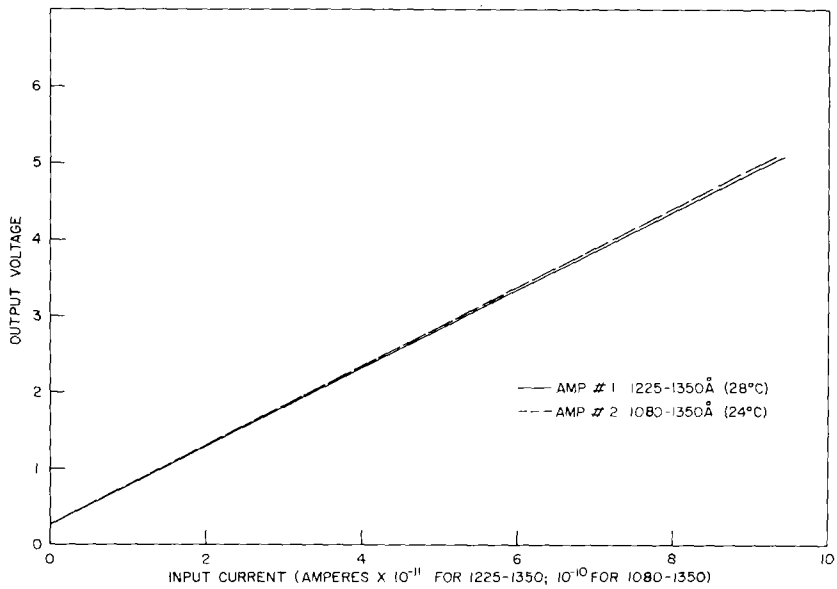


Fig. 30 - Voltage-current calibration curves for electrometer amplifiers used with the ultraviolet ionization chamber photometers

not possible to provide sufficient intensity of monochromatic ultraviolet in the laboratory, the calibration must be made with a fully open window. In flight, small apertures must be used to obtain on-scale readings of the solar flux. Because of this small aperture, any nonuniformity of the window material (LiF or $CaF_2$) will result in an unknown systematic error in the determination of absolute values of solar flux in these bands.

The second change was to place a negative polarizing voltage on the shell of the photometer. This change was made because separate amplifiers were used with each photometer, rather than using a single amplifier for both photometers, with midscale bias, as in the SOLRAD 8 instrument.

Both of these changes resulted in increased susceptibility of the photometers to surface photoemission and gas degradation by the very intense long-wavelength solar ultraviolet. Both ultraviolet experiments failed within two months after launch.

The amplifier calibration curves are presented in Fig. 30, and the angular response curves are in Figs. 31 and 32.

## 1 to 20 Å and 44 to 60 Å X-Ray Photometer Experiments

The 44 to 60 Å photometer experiment is basically the same as flown on previous SOLRAD satellites. Single-range electrometer amplifiers are used for both the 1 to 20 Å and 44 to 60 Å photometers. The calibration curves for these photometers are shown in Fig. 33, and the angular response curves appear in Figs. 34 and 35. Referring to Fig. 2, one sees that the 44 to 60 Å photometer is also sensitive below 20 Å. The 1 to 20 Å photometer was included in the complement of experiments to make a correction for this response. The method for making this correction is outlined in Appendix A.

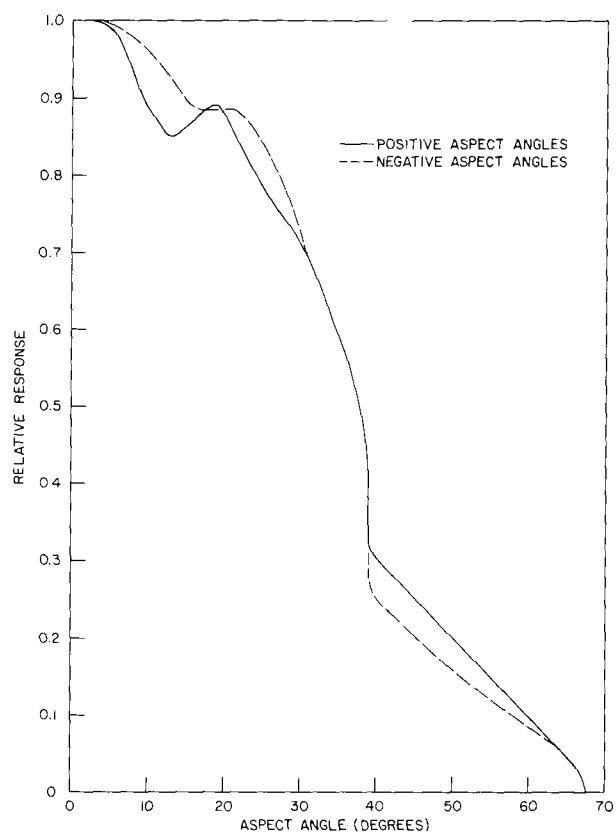


Fig. 31 - Angular response of the 1080 to 1350 Å ionization chamber photometer experiment. See Fig. 16 caption.

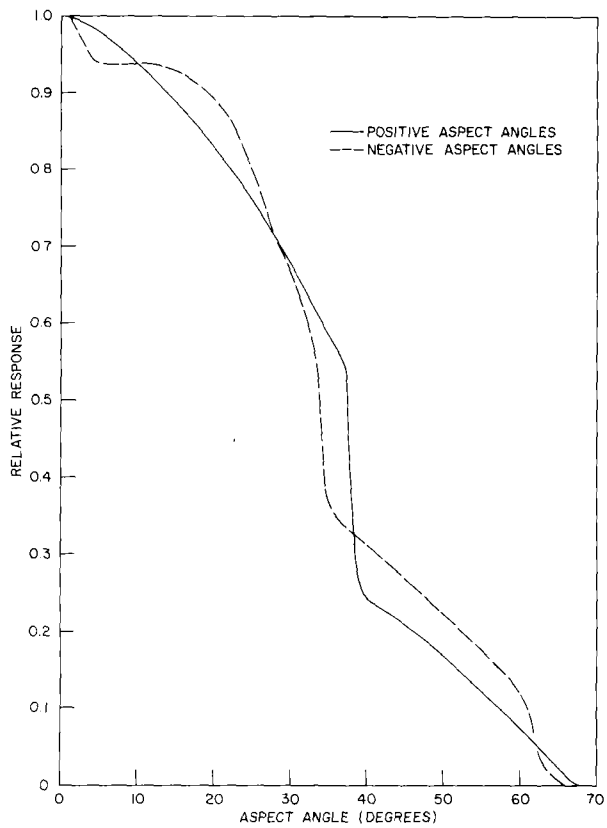


Fig. 32 - Angular response of the 1225 to 1350 Å ionization chamber photometer experiment. See Fig. 16 caption.

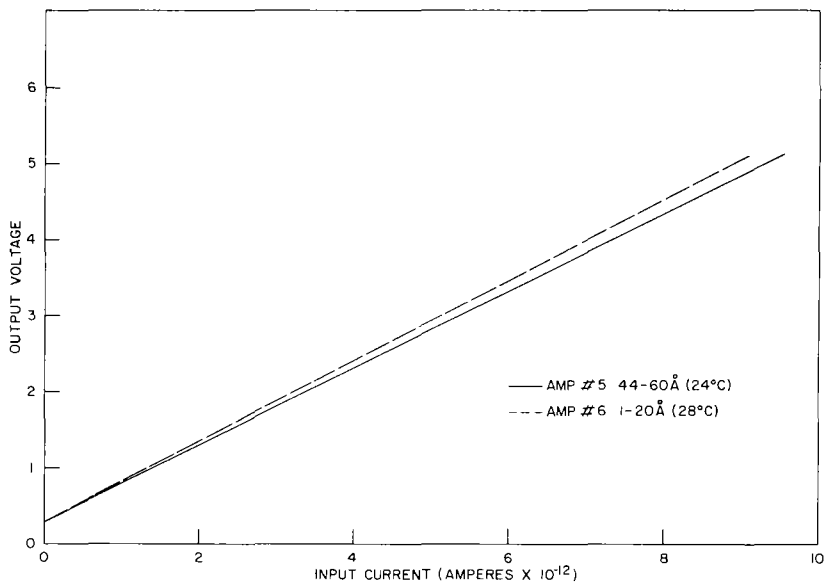


Fig. 33 - Voltage-current calibration curves for the electrometer amplifiers used with the 44 to 60 Å and 1 to 20 Å photometer experiments

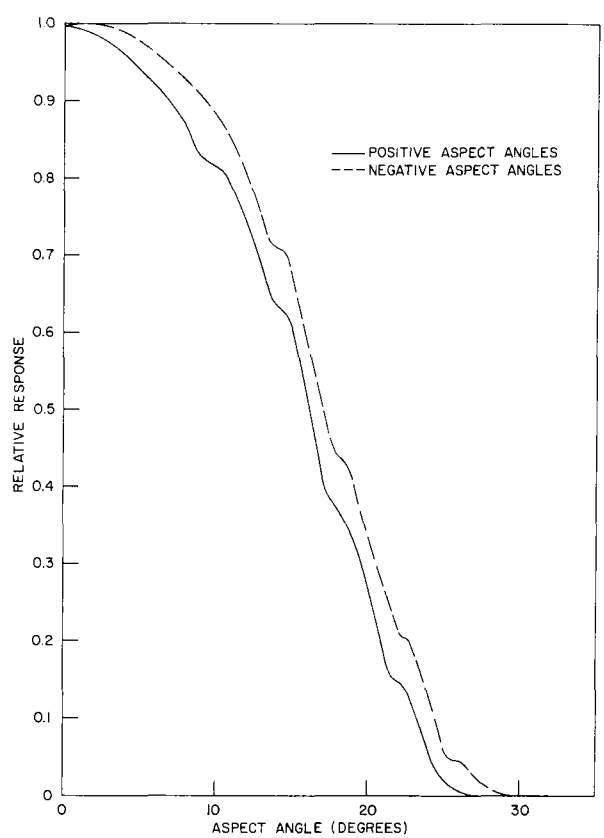


Fig. 34 - Angular response of the 44 to 60 Å ionization chamber (745). See Fig. 16 caption.

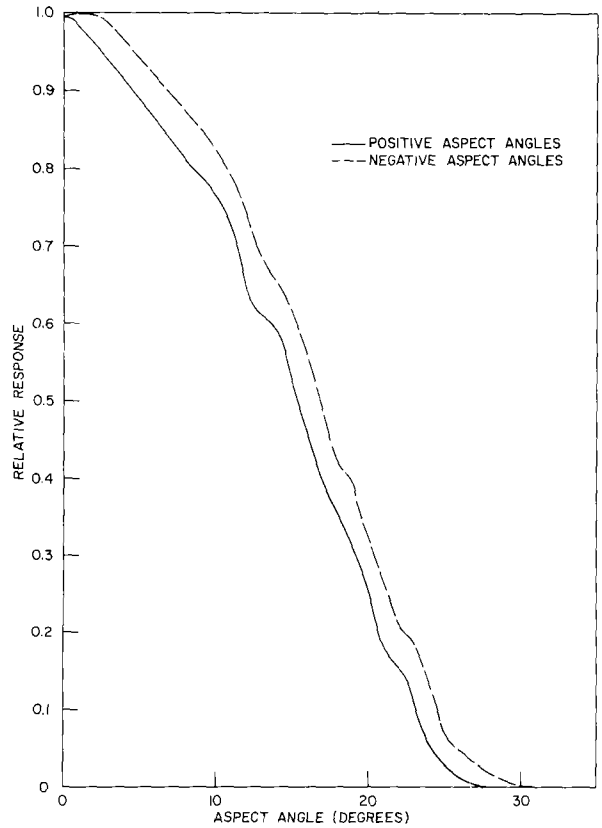


Fig. 35 - Angular response of the 1 to 20 Å ionization chamber photometer (732). See Fig. 16 caption.

Experiment Status Commutator

IRIG channel 3 contains information concerning experiment status and measurements of slowly varying engineering functions. Each measured quantity appears in one segment of a 32-segment commutator which is read out twice in the basic 32-sec data frame. The commutator readout appears in Fig. 36, and the segment allocations are given in Table 2.

## EXPERIMENT BLOCK DIAGRAM AND ANALOG OUTPUT FORMAT

The circuit block diagram is shown in Fig. 37. Each of the experiments has been described in the foregoing material, and no further explanation will be offered here. In Fig. 38 one data frame from an actual strip-chart recording has been reproduced to make clear the relationships among the data contained in the various channels.

## CONVERSION OF CURRENT OR COUNTING RATE TO FLUX VALUES

The conversion of the analog voltages scaled from the strip charts to energy flux may be made by means of the equation:

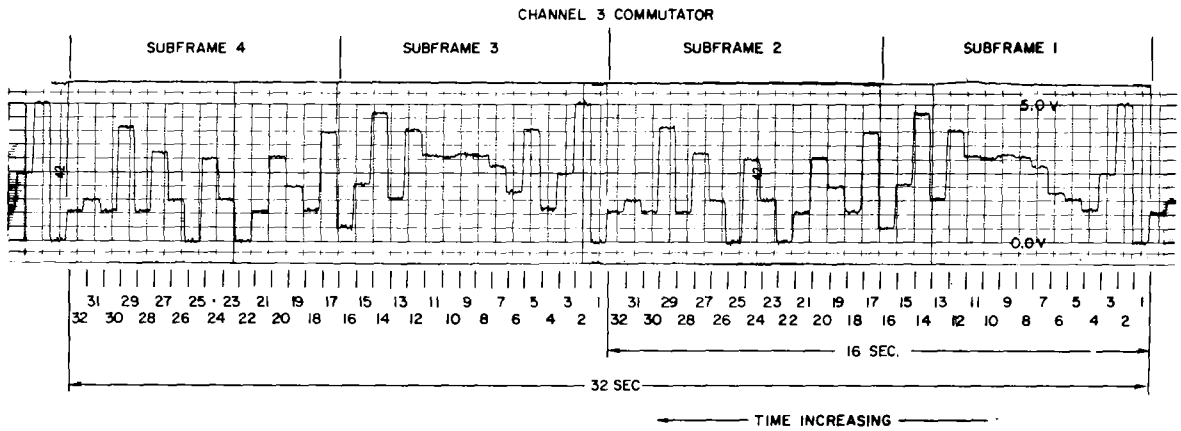


Fig. 36 - Reproduction of one data frame of the IRIG channel 3 commutator. See the text for a description of the format and Table 2 for commutator segment allocations.

$$F = \frac{K}{Am} V = CV$$

for the ionization-chamber experiments. In this equation

$F$ is in ergs $cm^{-2}$ $sec^{-1}$

$K$ is the detector conversion factor in ergs $sec^{-1}$ $amp^{-1}$

$A$ is the aperture area in $cm^2$

$m$ is the slope of the calibration curve in volts $amp^{-1}$.

Table 3 contains the numerical values of these parameters.

For the Geiger counter experiments a dead-time correction must be introduced. The conversion equation is:

$$F = \frac{K}{Am} V \cdot f(V) = CV \cdot f(V)$$

where $K$ is the conversion in ergs $count^{-1}$, $m$ is the slope in volts sec $count^{-1}$, and $f$ is the dead-time correction, which is a function of the counting rate or analog voltage output.

## NOTE ON ANGULAR RESPONSE CORRECTIONS

If one examines the measured angular response of the SOLRAD 9 photometers, a systematic difference in the response for positive and negative angles is observed. It has been concluded that this error was caused by an accidental displacement of the angular index wheel with respect to the mounting fixture for the photometer and magnet. The true angular-response correction must be made by adding 1.5 degree to the measured aspect angle for negative angles before reading the correction from the response curve. For positive angles, subtract one degree from the measured aspect angle before reading

Table 2
IRIG Channel 3 Commutator Segment Allocations

| Segment Number | Function | Description |
|---|---|---|
| 1 | Calibration | 0.0 Volt |
| 2 | Calibration | 5.0 Volts |
| 3 | Temperature | |
| 4 | Temperature | |
| 5 | Frame Ident. | First half data frame 30%<br>Second half 80% |
| 6 | Voltage | |
| 7 | Voltage | |
| 8 | Command | |
| 9 | Command | |
| 10 | Command | |
| 11 | Command | |
| 12 | Command | |
| 13 | Command | |
| 14 | Battery Pressure | |
| 15 | Attitude System | |
| 16 | Command | |
| 17 | Attitude System | |
| 18 | Memory | |
| 19 | Memory | |
| 20 | PCM Telemetry | |
| 21 | IR System | |
| 22 | 5A-5B Select | 5A on 0%; 5B on 84% |
| 23 | 5A-5B Range | Auto range 30%; Manual 80% |
| 24 | 5A-5B Range | Hi sens 0%; Lo sens 58% |
| 25 | 6A-6B Select | 6A on 0%; 6B on 84% |
| 26 | 6A-6B Range | Auto range 30%; Manual 80% |
| 27 | 6A-6B Range | Hi sens 0%; Lo sens 58% |
| 28 | 7A Status | On hi volt 20%; on lo volt 40%<br>Off 60% and 80% |
| 29 | 8A-8B Select | 8A on 30%; 8B on 80% |
| 30 | Exp 8 Status | On hi volt 20%; on lo volt 40%<br>Off 60% and 80% |
| 31 | Aspect Select | 9A on 30%; 9B on 80% |
| 32 | Exp 10 Status | 10A on 20% off 40%<br>10B on 60% off 80% |

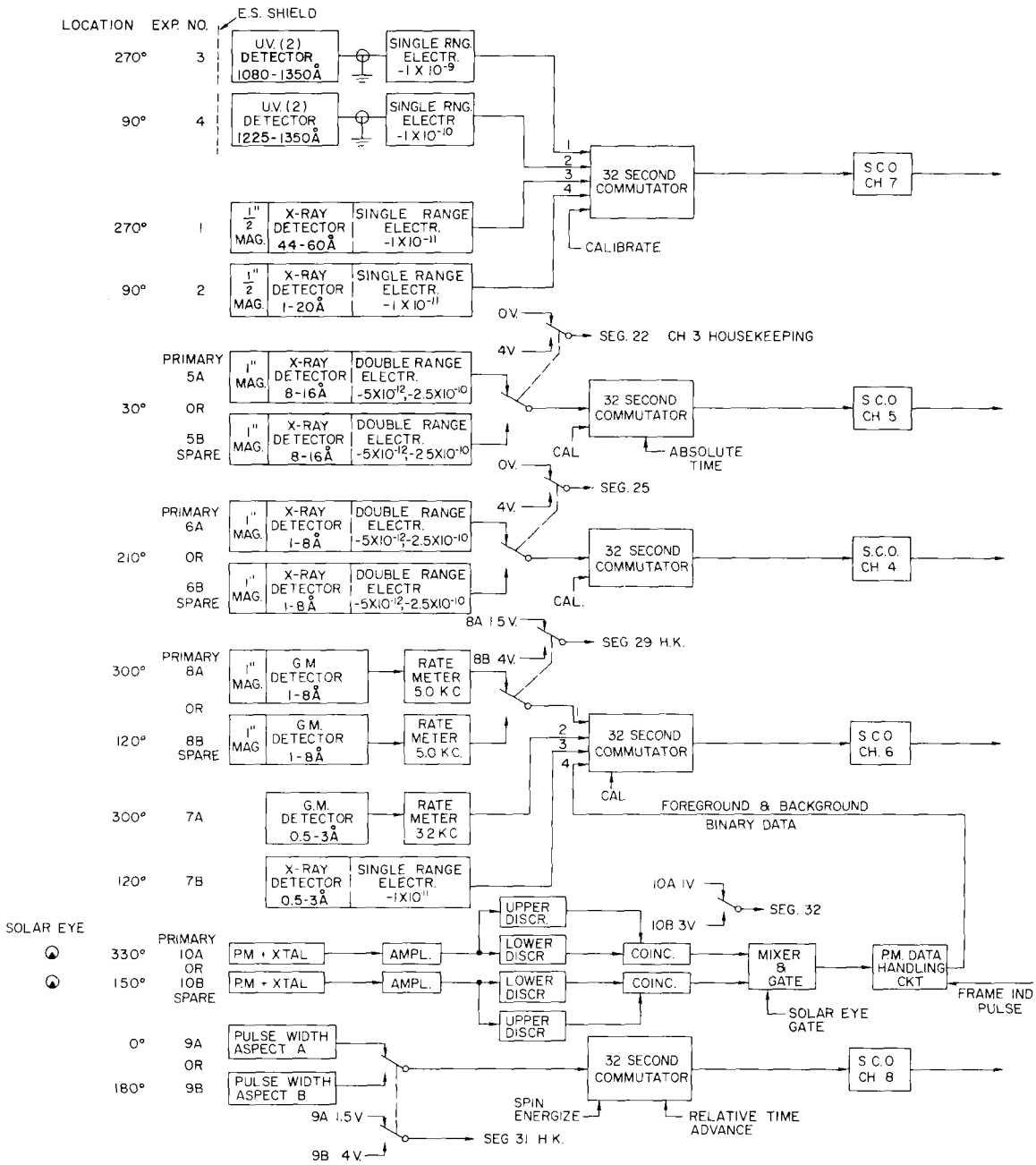


Fig. 37 - Block diagram of the SOLRAD 9 experiments

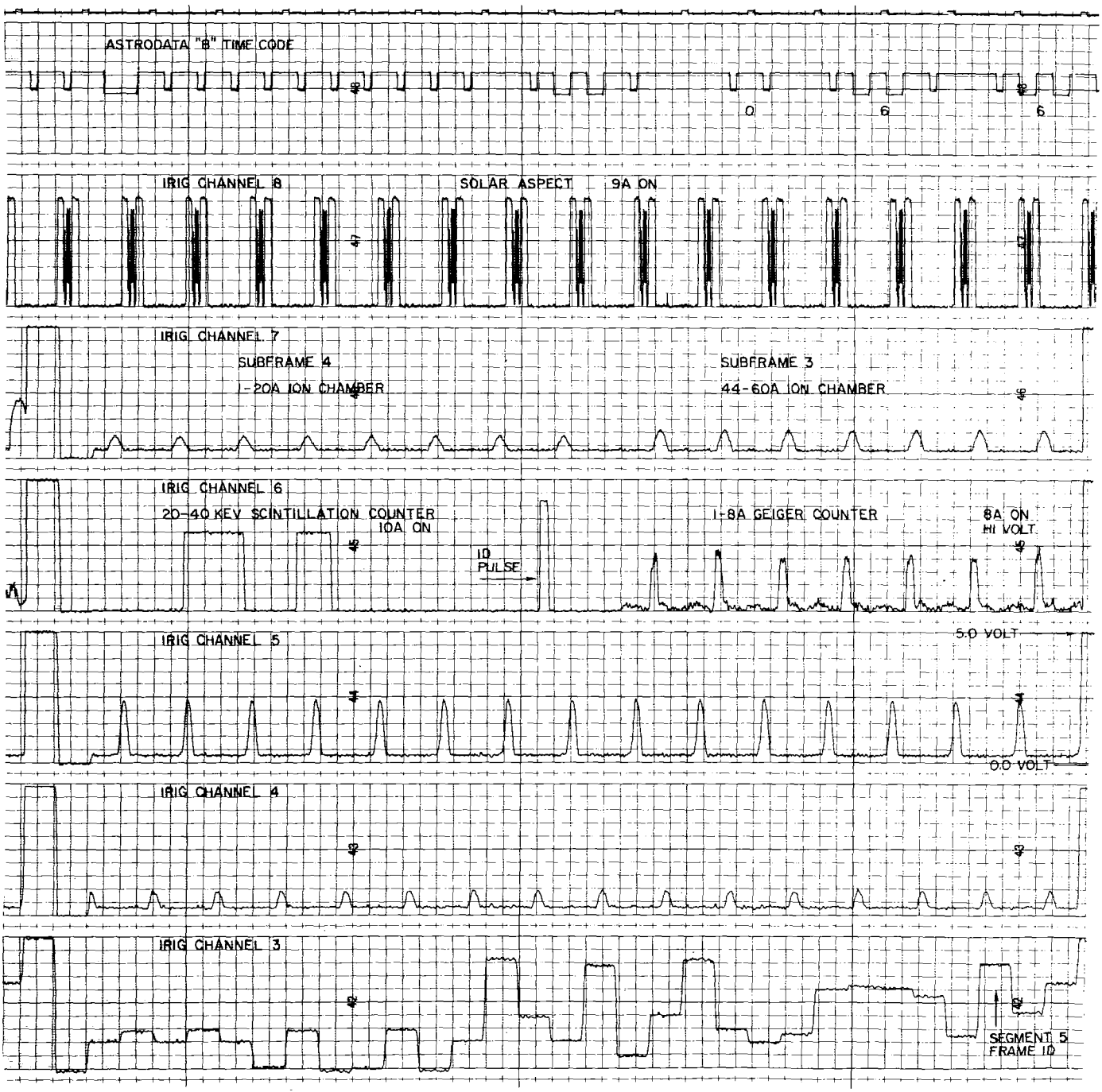


Fig. 38 - Reproduction of one dat:

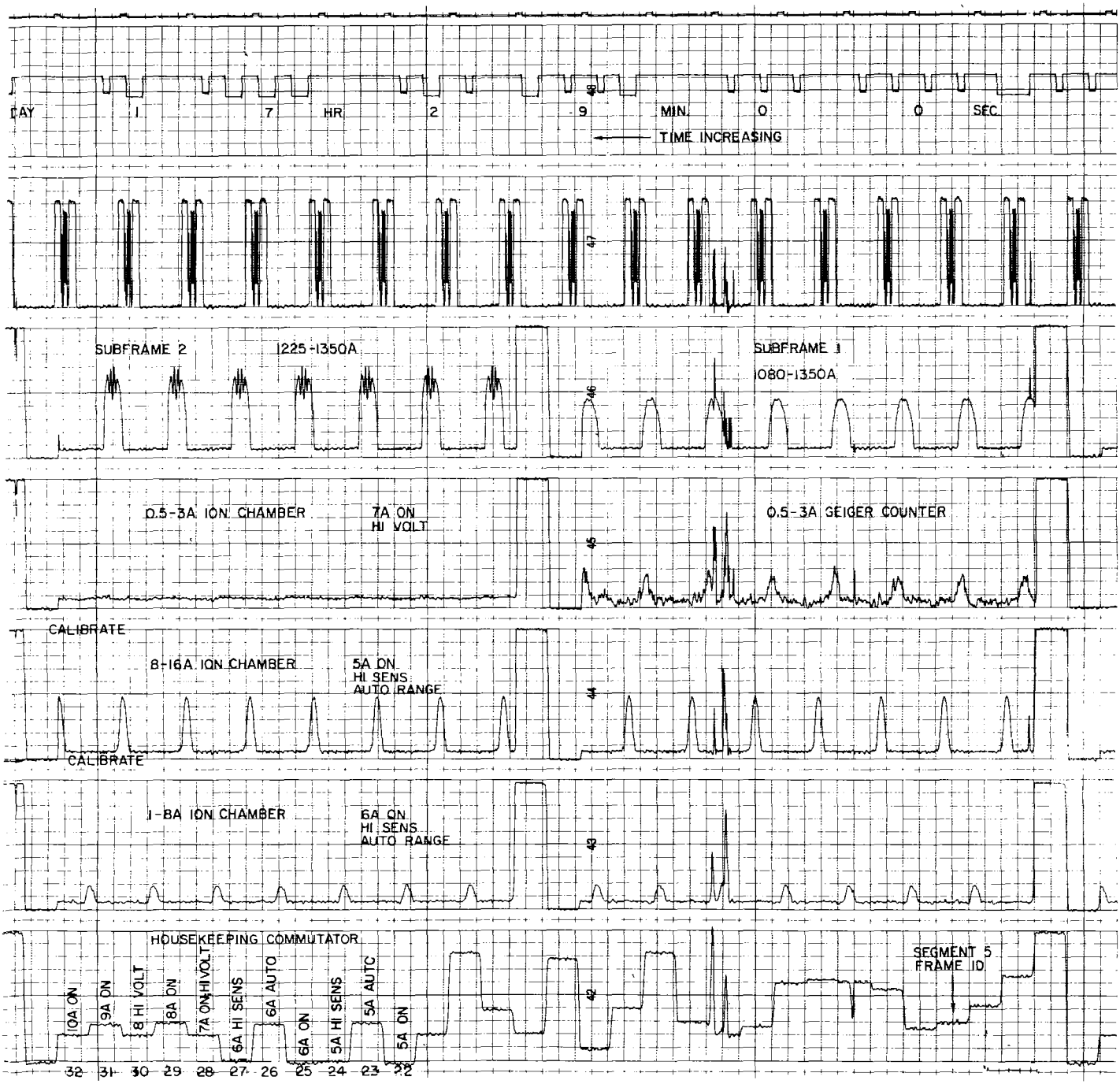


1 frame of all IRIG subcarrier channels

Fig 38-A

**This page intentionally left blank.**

Table 3
SOLRAD 9 Conversion Factors

| Experiment | Experiment Number | Scale | m (volts amp$^{-1}$)* | K (ergs sec$^{-1}$ amp$^{-1}$)† | A (cm$^2$)‡ | C (K/Am) | f (v) |
|---|---|---|---|---|---|---|---|
| 8-16 Å Primary | 5A | MS<br>LS | $1.03 \times 10^{12}$<br>$2.00 \times 10^{10}$ | $5.30 \times 10^{9}$<br>$5.30 \times 10^{9}$ | 0.78<br>0.78 | $6.63 \times 10^{-3}$<br>$3.41 \times 10^{-1}$ | |
| 8-16 Å Secondary | 5B | MS<br>LS | $1.06 \times 10^{12}$<br>$2.04 \times 10^{10}$ | $5.58 \times 10^{9}$<br>$5.58 \times 10^{9}$ | 0.78<br>0.78 | $6.78 \times 10^{-3}$<br>$3.53 \times 10^{-1}$ | |
| 1-20 Å | 2 | - | $0.53 \times 10^{12}$ | $4.8 \times 10^{9}$ | 0.174 | $5.23 \times 10^{-2}$ | |
| 44-60 Å | 1 | - | $0.51 \times 10^{12}$ | $1.91 \times 10^{10}$ | 0.174 | $2.18 \times 10^{-1}$ | |
| 1225-1350 Å | 4 | - | $0.51 \times 10^{11}$ | $4.58 \times 10^{8}$ | 0.044 | 0.206 | |
| 1080-1350 Å | 3 | - | $0.50 \times 10^{10}$ | $2.12 \times 10^{8}$ | 0.019 | 2.23 | |
| 0.5-3 Å IC | 7B | - | $0.52 \times 10^{12}$ | $7.87 \times 10^{8}$ | 5.28 | $2.89 \times 10^{-4}$ | |
| 1-8 Å GC | 8A | - | $8.77 \times 10^{-4}$ | $7.44 \times 10^{-8}$§ | 0.32 | $2.65 \times 10^{-4}$ | $\frac{1}{1-0.138V}$ |
| 1-8 Å GC | 8B | - | $8.72 \times 10^{-4}$ | $7.44 \times 10^{-8}$§ | 0.32 | $2.67 \times 10^{-4}$ | $\frac{1}{1-0.137V}$ |
| 40-80 kev | 10B | - | - | - | 10.2 | - | |
| 20-80 kev | 10A | - | - | - | 10.2 | - | |
| 1-8Å IC Primary | 6A | MS<br>LS | $1.04 \times 10^{12}$<br>$2.06 \times 10^{10}$ | $2.68 \times 10^{9}$<br>$2.68 \times 10^{9}$ | 1.16<br>1.16 | $2.23 \times 10^{-3}$<br>$1.12 \times 10^{-1}$ | |
| 1-8 Å IC Secondary | 6B | MS<br>LS | $1.03 \times 10^{12}$<br>$2.03 \times 10^{10}$ | $2.72 \times 10^{9}$<br>$2.72 \times 10^{9}$ | 1.16<br>1.16 | $2.28 \times 10^{-3}$<br>$1.16 \times 10^{-1}$ | |
| 0.5-3 Å GC | 7A | - | $1.37 \times 10^{-3}$ | $5.71 \times 10^{-8}$§ | 2.43 | $1.71 \times 10^{-5}$ | $\frac{1}{1-0.109V}$ |

*Slope of electrometer calibration curve
†Detector conversion constant
‡Effective window area
§Erg count$^{-1}$

the correction from the curve. Perhaps a better method would be to replot the aspect-correction curves, determining the position of zero degrees by folding the positive and negative sides onto each other so that the best fit is obtained.

## ACKNOWLEDGMENTS

The success of a major program such as SOLRAD depends on the efforts of many individuals. Among those who contributed to the preparation and launch of SOLRAD 9 are: P. G. Wilhelm and the Staff of the Satellite Techniques Branch, Application Research Division, L. Bowles, R. Grant, and R. Giroux of the Electronic Engineering Branch of ESD, and H. Chrisman and the Staff of the Operational Research Branch of ARD. R. G. Taylor of the Upper Air Physics Branch, Space Science Division was responsible for the preparation of the photometers, and Dr. C. S. Bowyer prepared the scintillation-counter experiment.

## Appendix A

## CORRECTION OF 44 TO 60 Å PHOTOMETER RESPONSE FOR RADIATION IN THE WAVELENGTH REGION BELOW 20 Å

Inspection of the wavelength response of the 44 to 60 Å photometer in Fig. 2 reveals immediately that this photometer will detect x-rays with wavelengths less than 20 Å with high efficiency.

Since it is known that solar flares are accompanied by large increases of x-radiation in this wavelength region, a method must be found to correct the 44 to 60 Å photometer response to radiation below 20 Å. The method we have chosen is to include in the satellite instrumentation a photometer sensitive mainly below 20 Å and whose efficiency in the region 8 to 20 Å closely matches that of the 44 to 60 Å photometer.

The efficiency of this photometer is also shown in Fig. 2.

The current produced in the 44 to 60 Å ionization chamber per unit wavelength interval $\Delta\lambda$ can be written

$$I_{1\lambda} = e\omega_1 a_1 B E_\lambda \epsilon_{1\lambda} \quad . \tag{A1}$$

The total current due to all wavelengths is just

$$I_1 = e\omega_1 a_1 B \sum_0^{70} E_\lambda \epsilon_{1\lambda} \Delta\lambda \quad . \tag{A2}$$

Similarly, we can write for the 1 to 20 Å ionization chamber

$$I_{2\lambda} = e\omega_2 a_2 B E_\lambda \epsilon_{2\lambda} \tag{A3}$$

and

$$I_2 = e\omega_2 a_2 B \sum_0^{70} E_\lambda \epsilon_{2\lambda} \Delta\lambda \quad . \tag{A4}$$

In these equations:

$e$ is the electronic charge, $1.6 \times 10^{-19}$ coulomb.

$\omega$ is the number of ion-electron pair produced per erg of incident energy

$\omega_1$ (Nitrogen) = $1.80 \times 10^{10}$ (Ref. 1)
$\omega_2$ ($CCl_4$) = $2.13 \times 10^{10}$*

*Determined by direct comparison with nitrogen in the laboratory.

$a$ is the open window area of the photometer $a_1 = a_2 = 0.174$ cm$^2$

$B$ is the dilution factor; it (Ref. 2) is the same for each of the photometers, since it describes the incident radiation and not the response of the photometer.

$E_\lambda$ is the energy input per unit wavelength interval in erg cm$^{-2}$ sec$^{-1}$ Angstrom$^{-1}$.

$\epsilon$ is the wavelength efficiency of the photometer. See Fig. 2.

The summation is made from 0 to 70 Å, the region in which the photometer is sensitive.

Now we wish to remove the current contribution below 44 Å from the 44 to 60 Å ionization chamber by means of the current measurement made with the 1 to 20 Å ion chamber. That is, we wish to make

$$I_1' - KI_2' = 0 \tag{A5}$$

where $I_1'$ and $I_2'$ are the integrated fluxes below 44 Å and $K$ is some constant independent of wavelength.

$$I_1' - KI_2' = eB\left[\omega_1 a_1 \sum_0^{44} E_\lambda \epsilon_{1\lambda} \Delta\lambda - K\omega_2 a_2 \sum_0^{44} E_\lambda \epsilon_{2\lambda} \Delta\lambda\right] . \tag{A6}$$

Since $K$ is a constant independent of wavelength, we would like to write

$$I_{1\lambda} - KI_{2\lambda} = 0 \tag{A7}$$

for the range 0 to 44 Å. But the wavelength response of the two ionization chambers differs because of the $Cl_K$, $Al_K$, and $N_K$ absorption edges which are not common to both chambers.

If we divide the 0 to 44 Å range into three regions, we can derive a value for $K$ which will satisfy the above condition to a good approximation. In the region 8 to 31 Å, there are no absorption edges not common to both chambers; therefore we can satisfy the equation

$$I_{1\lambda} - KI_{2\lambda} = 0 \quad (8 \text{ to } 31 \text{ Å}) \tag{A8}$$

almost perfectly.

Below 8 Å, where the response curves differ, we must depend on the sharply decreasing solar emission to render the response relatively unimportant. In addition, since the current collected in the ion chamber is a summation over contributions from radiation of all wavelengths local differences in absorption coefficient will tend to be unimportant. Thus we can require

$$I_{1\lambda} - KI_{2\lambda} \approx 0 \quad (0 \text{ to } 8 \text{ Å}) . \tag{A9}$$

Between 31 and 44 Å the window almost completely absorbs the solar radiation. Therefore, the contribution from this region can be neglected for both ionization chambers.

Using Eqs. (A2) and (A4), we can write

$$I_1 - KI_2 = eB\left[\omega_1 a_1 \sum_{0}^{70} E_\lambda \epsilon_{1\lambda} \Delta\lambda - K\omega_2 a_2 \sum_{0}^{70} E_\lambda \epsilon_{2\lambda} \Delta\lambda\right]. \tag{A10}$$

But because we have required that

$$I_1' - KI_2' \approx 0 \quad (0 \text{ to } 44 \text{ Å})$$

we can write

$$I_1 - KI_2 \approx eB\left[\omega_1 a_1 \sum_{44}^{70} E_\lambda \epsilon_{1\lambda} \Delta\lambda - K\omega_2 a_2 \sum_{44}^{70} E_\lambda \epsilon_{2\lambda} \Delta\lambda\right]. \tag{A11}$$

To determine the constant $K$, we return to Eq. (A6)

$$0 = eB\left[\omega_1 a_1 \sum_{0}^{44} E_\lambda \epsilon_{1\lambda} \Delta\lambda - K\omega_2 a_2 \sum_{0}^{44} E_\lambda \epsilon_{2\lambda} \Delta\lambda\right]$$

$$K\omega_2 a_2 \sum_{0}^{44} E_\lambda \epsilon_{2\lambda} \Delta\lambda = \omega_1 a_1 \sum_{0}^{44} E_\lambda \epsilon_{1\lambda} \Delta\lambda$$

$$K = \frac{\omega_1 a_1 \sum_{0}^{44} E_\lambda \epsilon_{1\lambda} \Delta\lambda}{\omega_2 a_2 \sum_{0}^{44} E_\lambda \epsilon_{2\lambda} \Delta\lambda}.$$

The window areas were made equal, so

$$K = \frac{\omega_1 \sum_0^{44} E_\lambda \epsilon_{1\lambda} \Delta\lambda}{\omega_2 \sum_0^{44} E_\lambda \epsilon_{2\lambda} \Delta\lambda} . \tag{A12}$$

From this result we see that $K$ can be obtained by matching the wavelength response curves $\epsilon_1$ and $\epsilon_2$ in the region below 44 Å for various gray-body spectral distributions. This has been done by a trial-and-error program, and a very close fit has been obtained for spectral distributions between 1 and 2 million degrees. For temperatures lower than $1 \times 10^6$ °$K$, the contribution due to radiation below 20 Å can be neglected. The value of $K$ thus obtained is 0.925.

Having determined the value of $K$, it is now necessary only to determine a conversion factor for calculating the 44 to 60 Å flux from the current difference $I = I_1 = KI_2$.

Following Ref. 2, the conversion factor can be written

$$CF = \frac{B \sum_{44}^{60} E_\lambda \Delta\lambda}{\sum_0^{70} (I_{1\lambda} - KI_{2\lambda}) \Delta\lambda} .$$

The denominator can be written in terms of known quantities as follows:

$$e\omega_1 a_1 B \sum_0^{70} E_\lambda \epsilon_{1\lambda} \Delta\lambda$$

$$- Ke\omega_2 a_2 B \sum_0^{70} E_\lambda \epsilon_{2\lambda} \Delta\lambda$$

$$= eBa \left[ \omega_1 \sum_0^{70} E_\lambda \epsilon_{1\lambda} \Delta\lambda \right.$$

$$\left. - K\omega_2 \sum_0^{70} E_\lambda \epsilon_{2\lambda} \Delta\lambda \right] .$$

Thus

$$CF = \frac{\sum_{44}^{60} E_\lambda \Delta\lambda}{ea \left[ \omega_1 \sum_0^{70} E_\lambda \epsilon_{1\lambda} \Delta\lambda - K\omega_2 \sum_0^{70} E_\lambda \epsilon_{2\lambda} \Delta\lambda \right]} . \tag{A13}$$

This equation is solved numerically for different temperature distributions. The results are

| T (°K) | CF* |
|---|---|
| $5 \times 10^5$ | $1.147 \times 10^{11}$ |
| $1 \times 10^6$ | $9.563 \times 10^{10}$ |
| $2 \times 10^6$ | $4.779 \times 10^{10}$ |

*units; erg $cm^{-2}$ $sec^{-1}$ $amp^{-1}$

## REFERENCES

1. Whyte, G.N., "Energy Per Ion Pair for Charged Particles in Gases," Rad. Res. 18(3):265-271 (Mar. 1963)

2. Kreplin, R.W., "Solar X-Rays," Ann. Geophys. 17(2):151-161 (Apr.-June 1961)

## Appendix B

## CORRECTION TO PHASE AND AMPLITUDE OF PHOTOMETER SIGNALS FOR SPIN RATE

Since the SOLRAD electrometer amplifier-photometer combinations have an effective time constant varying between 10 and 150 milliseconds, it is possible to experience both phase delays and attenuation of the output signals from the detectors.

This problem has been solved analytically and the results compared to measured responses of the photometers at different spin rates. Measurements have shown that the theoretical description of the response provides an adequate and useful description of the experiment behavior. The theoretical response is calculated by assuming an input function in the form of a series of terms $\sin^n \omega t$. The output response is given by

$$R = \frac{(-1)^{n/2}}{2^{n-1}} \left\{ \sum_{i=0}^{n/2-1} \frac{n!\,(-1)^i}{[1+(n-2i)^2 a^2]\; i!\,(n-1)!} \right.$$

$$[\cos (n-2i)\,\omega t + (n-2i)\,\omega \sin (n-2i)\,\omega t]$$

$$\left. + \frac{n!\,(-1)^{n/2}}{2\left(\frac{n}{2}!\right)^2} \right\}$$

for even values of $n$. Even values of $n$ represent pulses whose excursion from the base line is positive only.

From this equation the form of the output function can be calculated and compared directly with the input function in order to obtain the phase delay and output signal amplitude.

The value of $n$ is determined by an analysis of the signal obtained as the detector is slowly rotated through an x-ray beam. Although the experimental output will produce a single maximum during a rotation through 360 degrees, the mathematical representation of the signal, $\sin^n \omega t$, produces two maxima in 360 degrees. Therefore, the angle through which the detector is actually rotated must be divided by two to place the experimental signal and its mathematical representation on the same basis for comparison. The full-width-at-half-maximum ($\theta$) of the signal is measured in degrees based on two maxima per 360 degrees. Since the value of the half-maximum of a sine function is, of course, 0.5, we have

$$\sin^n \left( \frac{\pi}{2} \pm \frac{\theta}{2} \right) = 0.5$$

which converts to

$$n = \frac{\log 0.5}{\log \sin\left(\frac{\pi}{2} + \frac{\theta}{2}\right)} = \frac{\log 0.5}{\log\left(\cos \frac{\theta}{2}\right)} .$$

The value of $n$ obtained is then rounded off to the nearest even integer.

The value of $a$ is given by

$$a = \Omega\tau$$

where $\Omega$ is one-half of the spin rate of the satellite measured in radians per second and $\tau$ is the time constant of the detector and its associated electronics. The time constant is obtained by analysis of the decay of the output signal of the detector as the x-ray beam is suddenly interrupted. Since the detector and its electronics contain both capacitive and inductive elements, the analysis of the decay curve must be made in a region well removed from both the initial and final voltages. The relationship between two points $(V_i, t_i)$ on the decaying portion of the voltage vs time curve is

$$V_2 = V_1 e^{-(t_2 - t_1)/\tau}$$

which becomes

$$\tau = \frac{t_2 - t_1}{ln(V_1/V_2)} .$$

Therefore, the time constant is obtained from measured values of $V_2$, $V_1$, and $(t_2 - t_1)$.

Figure B1 shows the output signal for spin rates of zero and 1.5 rps for the amplifier whose output is most seriously distorted by the satellite spin. The abscissa is based on two maxima per 360 degrees, and so the phase lag of the signal peak measured from this plot must be multiplied by two to give the phase lag actually expected for this detector.

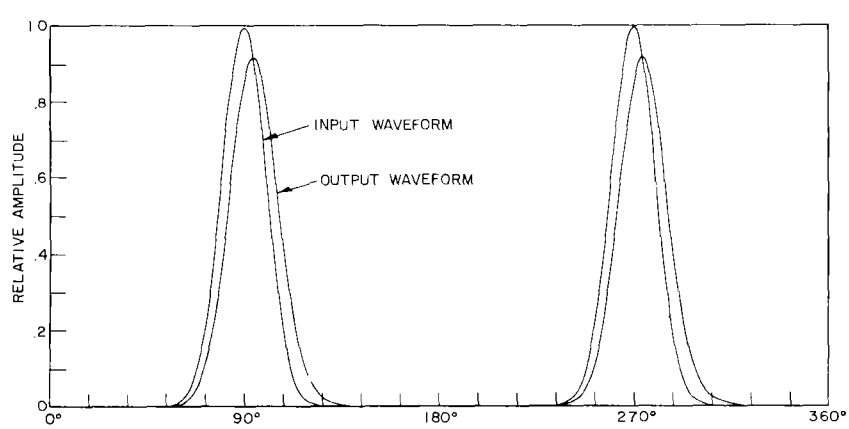


Fig. B1 - Illustration of the relationship between the input and output waveforms for the electrometer amplifier used in experiment 6, 1 to 8 Å, $\tau$ = 0.0177 sec, $n$ = 32, $a$ = 0.08336, 1.5 rev/sec

Tables B1 and B2 have been prepared to show the values of phase lag and amplitude to be expected from the SOLRAD 9 detectors for spin rates of 1 and 1.5 rps.

Table B1
SOLRAD 9 Detector Phase Lag and Amplitude,
Satellite Spinning at 1 rps

| Experiment | Phase Lag | Peak Ratio |
|---|---|---|
| 1 | 3.6° | 0.985 |
| 2 | <4.6° | >0.985 |
| 5 | 4.0° | 0.98 |
| 6 | 5.0° | 0.96 |
| 7A | <4.0° | >0.985 |
| 7B | 5.8° | 0.985 |

Table B2
SOLRAD 9 Detector Phase Lag and Amplitude,
Satellite Spinning at 1.5 rps

| Experiment | Phase Lag | Peak Ratio |
|---|---|---|
| 1 | 5.0° | 0.97 |
| 2 | 4.6° | 0.985 |
| 5 | 5.8° | 0.94 |
| 6 | 8.6° | 0.915 |
| 7A | <4.0° | >0.985 |
| 7B | 8.6° | 0.975 |

The phase lag gives the number of degrees that the peak of the pulse is displaced from the expected location of the peak on the analog strip charts. The peak ratio is the ratio of the peak height of the pulse from the spinning satellite to the peak height to be expected as the spin frequency is decreased toward zero.

An effort was made to provide a similar set of data for the GM counter experiments. The input waveshape was in this case trapezoidal, and the analysis was quite complicated. It was found that at a spin rate of 1.5 rps there was no decrease in the amplitude of the output signal. The phase delay was about equal to half the width of the input pulse. Because of the random nature of the counter output pulses, the wave shape of the input pulse is never ideal. Knowledge of the small correction for phase lag is of no practical importance.

Security Classification

## DOCUMENT CONTROL DATA - R & D

*(Security classification of title, body of abstract and indexing annotation must be entered when the overall report is classified)*

| | |
|---|---|
| 1. ORIGINATING ACTIVITY *(Corporate author)*<br>Naval Research Laboratory<br>Washington, D.C. 20390 | 2a. REPORT SECURITY CLASSIFICATION<br>Unclassified<br>2b. GROUP<br>— |

3. REPORT TITLE

THE NRL SOLRAD 9 SATELLITE, SOLAR EXPLORER B, 1968-17A

4. DESCRIPTIVE NOTES *(Type of report and inclusive dates)*

A report on one phase of the problem; work is continuing.

5. AUTHOR(S) *(First name, middle initial, last name)*

Kreplin, Robert W., and Horan, Donald M.

| | | |
|---|---|---|
| 6. REPORT DATE | 7a. TOTAL NO. OF PAGES<br>50 | 7b. NO. OF REFS<br>2 |
| 8a. CONTRACT OR GRANT NO.<br>NRL Problem A01-20<br>b. PROJECT NO.<br>A37538/6521/F019-02-02<br>c.<br>d. | 9a. ORIGINATOR'S REPORT NUMBER(S)<br>NRL Report 6800<br>9b. OTHER REPORT NO(S) *(Any other numbers that may be assigned this report)* | |

10. DISTRIBUTION STATEMENT

This document has been approved for public release and sale; its distribution is unlimited.

| | |
|---|---|
| 11. SUPPLEMENTARY NOTES | 12. SPONSORING MILITARY ACTIVITY<br>Department of the Navy<br>(Naval Air Systems Command)<br>Washington, D.C. |

13. ABSTRACT


The NRL SOLRAD 9 satellite, launched March 5, 1968, carried instruments to measure solar radiation in the x-ray region from 0.1 to 60 Angstroms and in the far-ultraviolet from 1080 to 1350 Angstroms. These spectral regions are covered by a number of band-sensitive ionization-chamber photometers, Geiger counters, and scintillation counters. These bands are: 20 to 80 kev (0.15 to 0.6 Å); 40 to 80 kev (0.15 to 0.3 Å); 0.5 to 3 Å; 1 to 8 Å; 8 to 16 Å; 1 to 20 Å; 44 to 60 Å; 1080 to 1350 Å; and 1225 to 1350 Å. An aspect sensor was also included to measure the angle between the solar direction and view direction of the photometers for correction of photometer measurements in case of failure of the attitude-control system.

The satellite transmits its x-ray and ultraviolet measurements in real time via an FM/AM telemetry system operating in the 136-MHz band. The standard IRIG subcarrier channels 3 through 8 carry the output of the various photometers and associated housekeeping data.

Individual scientists and institutions have been invited through COSPAR to receive and use the real-time transmission of x-ray and ultraviolet measurements in their own research programs.

This report carries a full description of each instrument aboard the SOLRAD 9 spacecraft and all calibration data required to reduce the telemetered measurements to x-ray and ultraviolet flux values.


DD FORM 1 NOV 65 1473 (PAGE 1)



S/N 0101-807-6801

Security Classification

Security Classification

| 14. KEY WORDS | LINK A ROLE | LINK A WT | LINK B ROLE | LINK B WT | LINK C ROLE | LINK C WT |
|---|---|---|---|---|---|---|
| Satellites | | | | | | |
| Solar satellites | | | | | | |
| SOLRAD 9 | | | | | | |
| SOLAR EXPLORER B | | | | | | |
| Solar x-rays | | | | | | |
| Telemetry | | | | | | |
| 1968-17A | | | | | | |

DD FORM 1 NOV 65 1473 (BACK)
(PAGE 2)



Security Classification